東北大学機関リポジトリ
TOUR
Tohoku University Repository

Analysis of myogenic and adipogenic precursor cell features in rotator cuff tear with fatty infiltration

	Koide Masashi
	Tohoku University
	11301 17411
URL	http://hdl.handle.net/10097/00122089

博士論文

Analysis of myogenic and adipogenic precursor cell

features in rotator cuff tear with fatty infiltration

脂肪変性した腱板筋における筋・脂肪前駆細胞の解析

東北大学大学院医学系研究科医科学専攻

外科病態学講座整形外科学分野

小出　将志

Abstract

Rotator cuff tear is a common disease in elderly patients that leads to shoulder weakness, pain, and disability in the activities of daily living. Some patients with massive rotator cuff tears have an unacceptable clinical outcome because of muscle atrophy and fatty infiltration. The satellite cell has central role of muscle regeneration, however, there are few reports about human muscle. Multi-photon microscopy has been a popular method for biological imaging. Multi-photon imaging can visualize deep tissues up to approximately 1 mm with 3-dimensional (3D) micro-structure. Although there have been a few reports for multi-photon imaging of skeletal muscles in animals, there are no reports for humans. The purpose of this study was to observe muscle tissues from patients with rotator cuff tears by multi-photon imaging to evaluate microstructural changes and to compare *in vivo* features of human myogenic and adipogenic precursors in the rotator cuff muscles in both torn supraspinatus (SSP) and intact subscapularis (SSC) tendons.

Muscle biopsies were obtained from the SSP and SSC muscles from 19 patients. For the flow cytometry, the muscle tissue samples were digested and stained with antibodies. The myogenic precursors were defined as

CD11b-CD31-CD34-CD45-CD56+ cells, whereas the adipogenic precursors were defined as CD11b-CD31-CD45- Platlet-Derived Growth Factor Receptor alpha (PDGFRα)+ cells. After these precursors were sorted, they were seeded in plates with growth media. The area of muscle and fat tissues of magnetic resonance imaging (MRI) conducted before the surgery was compared with the population of these precursors. In the culture of myogenic precursors, the potential of myogenic differentiation was evaluated. Gene and protein expressions related to myogenic maturation were analyzed by DNA microarray. For the multi-photon imaging, the muscle tissues were observed as a whole block stained with BODIPY, Hechst33342, and Isolectin.

In the analysis of flow cytometry, there was a positive correlation between the population of precursors with the index of muscle/fat area of the MRI. In the culture of myogenic precursors, there was myotube formation in both SSC and SSP groups. In the DNA microarray analysis, myosin related gene expressions in the SSP group was higher than the SSC group. In the multi-photon imaging, clear 3D image of adipogenic tissue in the muscle was observed.

The human satellite cells from the SSP muscle with fatty infiltration maintained intrinsic myogenic potentials. The population of adipogenic precursors was distinct in the torn SSP muscle compared to the intact SSC muscle.

Introduction

A rotator cuff tear is a common cause of shoulder weakness and pain in elderly patients, which causes difficulties in activities of daily living[5,20]. The shoulder joint is a ball-and-socket joint and the upper arm is kept in the shoulder socket by the rotator cuff[13]. The rotator cuff is a network of four muscles that come together as tendons to form a covering around the head of the humerus[14] (Fig. 1). The rotator cuff attaches the humerus to the shoulder blade and helps to lift and rotate the arm. It has been estimated that 30% of the general population over 60 years has a full thickness rotator cuff tendon tear[54]. When the symptoms are severe or recalcitrant, surgical repairs are recommended. Small or medium sized rotator cuff tendon tears are a good indication for surgical repairs with excellent clinical results. However, patients with large or massive rotator cuff tendon tears do not have good clinical results after surgeries because of poor quality of the tendons or affected muscles[16]. Fatty infiltration and atrophy of the rotator

cuff muscles are one of the most important factors which correlate with poor functional outcome after surgeries [20,31,36].

Similarly in other muscular diseases of sarcopenia or muscular dystrophies[44], severely damaged rotator cuff tendons induce severe muscle atrophy with fatty infiltration and they were occupied with adipocytes[16,42]. Sarcopenia has been defined as an age related involuntary loss of skeletal muscle mass and strength[50]. Despite its high prevalence, clear consensus and definition have not been developed[8]. Causes of sarcopenia include declines in hormones and numbers of neuromuscular junctions, increased inflammation, declines in activity, and inadequate nutrition[57]. Muscular dystrophy is a group of muscle diseases that weaken the musculoskeletal system and hamper locomotion[3]. Although physiotherapy, aerobic exercise, and low-intensity catabolic steroids can help to maintain muscle tone, no specific treatment or cure for muscular diseases are known. Fatty infiltration into skeletal muscles has been regarded as muscle degeneration including impairments of myogenic function of satellite cells[46,42].

The muscle satellite cell is defined as a typical muscle stem cell that exhibits self-renewal and myogenic differentiation capacities[1,9,30], and characterized by the cell

surface antigen of CD56 positive in human. Satellite cells are generally quiescent and locate between the basal lamina and sarcolemma of the skeletal muscle fibers[64]. However, muscular damages rapidly induce satellite cell activation and accelerate their proliferation and repair/regeneration of the damaged muscles[6]. Although human and mouse satellite cells express similar markers, it has been difficult to determine whether their phenotype and functions are equivalent. This is mostly due to a difficulty in isolating quiescent human satellite cells and the lack of specific markers for their unequivocal identification[6]. Although CD56 is not expressed by quiescent satellite cells and begins to be expressed only after denervation or differentiation in mouse[27], both quiescent and activated human muscle satellite cells express CD56[48]. Therefore, this molecule has been extensively used as a marker for identification and isolation of satellite cells from human muscles[4,55,59]. Several previous reports have indicated that satellite cells maintain an ability for muscle regeneration regardless of the severity of rotator cuff tendon tears[37].

Adipocytes are originated from mesenchymal stem cells[30,56]. Uezumi et al. reported that their progenitors are characterized with CD45-/CD31- and Platelet-Derived Growth Factor Receptor alpha (PDGFRα) positive expressions in the

interstitium regions of human skeletal muscles[55]. PDGFRα positive cells are distinct

from myogenic progenitor cells, because of their adipogenic potentials[55]. However, an

influence of pathophysiological conditions on the adipogenic precursor cells in human

skeletal muscles has not been clear[45,47,55].

Multi photon microscopy is now becoming a popular method for biological

imaging and evaluation. Because multi-photon imaging is able to reveal ultra-structures

of elastin and collagen fibers without staining, it has been widely come to use in

cardiovascular and dermatological researches[10,12]. Chen et al. reported multi-photon

imaging study of the morphological and quantity changes of collagen and elastic fiber

components in keloid disease[10]. Cui et al. reported aortic and cutaneous elastin and

collagen morphology using multi-photon imaging[12]. Because multi-photon imaging can

visualize the deep tissue up to approximately 1 mm with 3-dimensional (3D)

micro-structure, twisted collagen fibers, blood vessels, muscle sarcomere, and

infiltration of adipogenic tissues can be easily recognized. Hunt et al. reported stained

polyubiquitin within muscle fibers with whole mount immunostaining of Drosophila

skeletal muscle[25]. Rothstein et al. reported the structure of sarcomere of skeletal muscle

in in-vivo imaging of the tibialis anterior muscles of mouse and rabbit using

multi-photon imaging[49]. Although there have been a few reports for multi-photon

imaging of skeletal muscles in animals[25], there is no reports for humans.

Purpose

The purpose of this study was to observe muscle tissues from patients with rotator cuff tears by multi-photon imaging to evaluate microstructural changes and to compare *in vivo* features of human myogenic and adipogenic precursors in the rotator cuff muscles in both torn supraspinatus (SSP) and intact subscapularis (SSC). The correlation between the ratio of adipogenic/myogenic progenitor cells and a degree of muscle atrophy evaluated by magnetic resonance imaging (MRI) was examined. Furthermore, we compared gene expression patterns of the satellite cells in the SSP and SSC muscles by DNA microarray analysis and compared gene expressions of regeneration.

Materials and Methods

Patients

The protocols of this study were approved by Tohoku University Hospital's Institutional Review Board (approved number; 2014-1-703) and signed consent was obtained from all the participants. From October 2014 to December 2015, we performed an arthroscopic rotator cuff repair in 19 patients with failed conservative treatments (Table 1). All the patients had no tears in the SSC tendon evaluated by both MRI and arthroscopic findings. There was no muscular disease, neurovascular problem, paralysis, and trauma in all of them. Muscle biopsies (approximately 300 mg) were obtained from the middle of the SSP and SSC muscles by using arthroscopic forceps (Fig. 1). The site of the muscle biopsy was the muscle belly, which is far proximally to the tendon. The average age was 64.5 ± 8.0 years (47-76 year; 10 males and 9 females).

Multi-photon Imaging

Samples of the SSP and SSC muscles from 6 patients were used for multi-photon imaging. The muscle tissues were collected and immediately fixed with 4%

paraformaldehyde in 0.1M phosphate-buffer, pH7.4, containing 18% sucrose for overnight. Then the sample was washed by PBS three times and stained with BODIPY 558/568 C12 (Final concentration: 5 μM, Life Technologies, Carlsbad, CA), Hoechst 33342 (Final concentration: 40 μM, Dojindo Molecular Technologies, Inc, Kumamoto, Japan), and Alexa Fluor 488-conjugated isolectin GS-IB4 (Final concentration: 10 μg/ml, Life Technologies) for 30 min at 4°C. Imaging experiments were performed with a multi-photon imaging systems with an upright microscope (A1R-MP+, Nikon Corporation, Tokyo, Japan) equipped with a Ti-sapphire laser (Mai-Tai DeepSee, Spectra-Physics, Santa Clara, CA), and a 25x water objective lens (NA 1.10). Excitation was performed at 920 nm, and all signals were detected via GaAsP type non-descanned detectors 425–475 nm for SHG signals and Hoechst 33342 fluorescence (blue channel), 500–550 nm for Alexa Fluor 488 fluorescence (green channel) and 601–657 nm for BODIPY 558/568 fluorescence (red channel). Image stacks consisting of 280 optical sections with 2 μm z-steps were acquired, and 3D reconstruction was performed with NIS element (Nikon).[41].

Cell Isolation and Proliferation

Blood cells in the sample were washed out with normal saline and transferred to

DMEM (sterilized, Wako Pure Chemicals Industries, LTD, Japan) supplemented with

1% penicillin-streptomycin. The tissue was minced and digested with 0.2% collagenase

(Wako) and 0.1% DNase I (Sigma-Aldrich, St. Louis, MO) for 1 hr at 37°C. Digested

muscle tissues were added in sterilized PBS and filtered through a 70 μm cell strainer

(Becton, Dickinson and Company, Franklin Lakes, NJ) and then centrifuged at 700x g

for 20 min. The pellets were resuspended in 1 ml staining solution consisted with PBS

and 1 % bovine serum albumin (Sigma-Aldrich, St. Lois, MO), and then stained with Fc

receptor blocking solution (Human TruStain FcX, 1:20 in staining buffer; Biolegend,

San Diego, CA) for 10 min, and stained with monoclonal antibodies as follows:

FITC-conjugated anti-CD45 (1:20, Biolegend, clone HI30), FITC-conjugated

anti-CD11b (1:20, Biolegend, clone ICRF444), FITC-conjugated anti-CD31 (1:20,

Biolegend, clone WM59), PE/Cy7-conjugated anti-CD34 (1:20, Biolegend, clone 581),

APC-conjugated anti-CD56 (1:20, Biolegend, clone MEM-188), PE-conjugated

anti-PDGFRα (1:20, Biolegend, clone 16A1) (Table 2). After 45 min incubation on ice,

the cell suspension was washed with staining solution and centrifuged for 5 min at 700x

g twice. Human satellite cells were defined as single live mononuclear

CD11b-CD31-CD34-CD45-CD56+ cells, and adipogenic precursors were as

CD11b-CD31-CD45-PDGFRα+ cells[55,4]. Fluorescence activated cell sorting (FACS) was conducted with BD FACS ARIA II flow cytometer (Becton, Dickinson and Company), and analyzed with Flowjo software (Flowjo, LLC, Ashland, OR). These cells were seeded on the Matrigel (Corning Inc., Corning, NY) coated 24 well chamber slides with growth media consisting of DMEM/Ham's F10 mixture supplemented with 20% fetal bovine serum (FBS), 1% penicillin-streptomycin, 10% chicken embryonic extract (United States Biological, Inc., Salem, MA), 2.5 ng/ml bFGF (Thermo Fischer Scientific, Inc., Waltham, MA), and incubated at 37 °C under a 5% CO_2 atmosphere. After reaching at 80-90% of confluence, adhered cells were dissociated by 1 mM EDTA and transferred to a new Matrigel-coated 10 cm dish for passage. Because adipogenic precursors didn't have sufficient proliferation for the use of next steps, only the satellite cells were kept in liquid nitrogen.

Immunostaining

The satellite cells are seeded in the Matrigel-coated 6 well plates. Myogenic differentiation was induced by switching growth medium to DMEM/Ham's F10 mixture supplemented with 5% horse serum and 1% penicillin-streptomycin. The

differentiation medium was changed every 24 hrs. For the immunofluorescent staining experiment, cells were grown on Matrigel-coated 22-mm glass coverslips (Matsunami C022221, Osaka, Japan) in 6 well plates. After the treatments, the cells were washed in PBS and fixed with 2% paraformaldehyde/PBS containing 0.1% Triton X-100 for 20 min. The cells were washed, and then blocked in PBS containing 5% calf serum plus 1% BSA for 1 hr at room temperature. Anti-human myosin heavy chain antibody (R&D Systems, MAB4470, Minneapolis, MN) and Alexa Fluor 594-conjugated anti-mouse IgG secondary antibody (Thermo Fischer Scientific, Waltham, MA) were used at 1:100 and 1:1000 dilutions in 1% BSA/PBS, respectively, and the samples were mounted on glass slides with Vectashield (Vector Laboratories, Burlingame, CA). The cells were observed with a confocal fluorescence microscope (Olympus Fluoview FV-1000, Tokyo, Japan) and associated application program ASW Ver. 1.3 (Olympus, Tokyo, Japan). Images were then imported into Adobe Photoshop 6.0 (Adobe Systems, Inc., San Jose, CA) and Image-Pro Plus (Media Cybernetics, Inc., Rockville, MD) for processing. The differentiation of the muscle precursor cells was evaluated by the number of myotubes and the fusion rate of nuclei in myotubes.[37] The number of myotubes, defined as nuclei inside and myosin heavy chain positive, were counted within a 500-μm × 500-μm area by each number of nuclei inside the cell. The fusion

rate which was the number of nuclei in myotubes (DAPI) was evaluated by 3 groups as follows; the number of nuclei of 1-3, 4-10, and more than 10. At least five fields were counted for each sample under 200× microscopic magnification. For all the microscopic analyses, at least three independent experiments were performed for each condition[2].

MRI Quantification

Originally, Goutallier et al. graded fatty infiltration of the rotator cuff muscles for 5 stages by computed tomography but modified for MRI analysis by Fuchs et al. [17,21] as follows; 0, normal; 1, some fat streaks; 2, fatty degeneration of less than 50%; 3, 50% fatty muscle atrophy; and 4, fatty infiltration of more than 50%. A muscle/adipose tissue ratio of the SSP and SSC muscles was evaluated with MRI (Hitachi Medical Corporation, Japan) before arthroscopic surgery (Fig.2). This protocol was used to analyze the most lateral sagittal-oblique image where the acromion, coracoid, and scapular body were all visible, together with the next 2 consecutive lateral images[5] (Fig. 3).

DNA MicroarrayAnalysis

Two pairs of satellite cells derived from muscle samples (Patient#1 & 7, shown in Table1) were used for DNA microarray analysis. After a treatment with DNase I (Invitrogen, Carlsbad, CA), RNAs were amplified using Amino Ally MessageAmp II aRNA Amplification Kit (Ambion, Austin, TX) and labeled with Cy3 and Cy5. Whole Human Genome Microarray Kit 4×44 K (Agilent, Santa Clara, CA) was applied to the Cy3- and Cy5-labeled amplified RNAs, which were then competitively hybridized at 65°C for 17 hrs. The microarray was scanned with GenePix 4000B (Molecular Devices, Downingtown, PA). The scanned image was analyzed with GenePix Pro 6 software (Molecular Devices)[23,61]. To characterize gene expression profiles, probes whose expressions changed by more than 2-fold upregulation or less than one-half of downregulation in the satellite cells from the SSP compared with the satellite cells from the SSC were selected[23,60]. Based on Gene Ontology database (http://www.geneontology.org), I performed Gene Ontology (GO) analysis and classified differential gene functions[39]. P-values less than 0.05 was considered as the statistical significance of GO term enrichment.

Statistical Analysis

All statistical analyses were performed with SPSS version 23.0 (SPSS Japan Inc., Tokyo, Japan). Experimental values are given as the mean ± standard error of the mean (SEM). Statistical significance was assessed either by a Mann-Whitney U-Test (for comparing two means). P-values less than 0.05 were considered as statiscilay significant.

Results

Structural Changes of Atrophied and Normal Muscles

The SSC and SSP muscles obtained from the same patient were observed with multi-photon imaging. Muscle fibers can be recognized with green auto-fluorescence without staining (Fig. 4A). However, adipogenic tissues could not be recognized without staining (Fig. 4B). There was no adipogenic tissue within muscle fibers in the SSC group. The collagen fibers surrounding the adipogenic tissue could be seen with blue signal, which is called second harmonic generation. Under stained condition with BODIPY 558/568 C12, Hoechst 33342 and Alexa Fluor 488-conjugated isolectin GS-IB4, the nuclei of cells stained with Heachst 33342 with blue signal were scattered around the sarcomere (Fig. 5A). The adipogenic tissue stained with BODIPY could be clearly visualized with multi-photon imaging (Fig. 5B). Although the capillary vessels were stained with isolectin for green, twisted shape was different from sarcomeres. The adipose tissue was not localized near the blood vessels in the SSC muscle tissues (Fig. 6A), but the SSP muscle tissues contained inter-muscular proliferation of collagen fibers with blue signal, which includes adipose tissues stained with BODIPY for red

(Fig. 6B). The fatty infiltration in the muscle tissue was observed only in the SSP muscle.

Proportion of Myogenic/Adipogenic Precursor Cells

The satellite cells defined as single live mononuclear CD11b-CD31-CD34-CD45-CD56+ cells were sorted by gating strategy (Fig.7). The dead cells stained with DAPI and doublets were removed. The negative set included blood markers of CD11b and CD45, the endothelial marker of CD31 and CD34. The gate was set by negative control. The adipogenic precursors cells defined as CD11b-CD31-CD45-PDGFRα+ cells were also sorted by gating strategy (Fig. 8). The population of myogenic and adipogenic precursors was analyzed with flowcytometry (Fig. 9). The satellite cells constituted 0.17% ($\pm$0.036% SEM) and 0.12% ($\pm$0.027% SEM) of the total events in the SSC or SSP muscles (n=19 in each group) were collected (Fig. 9A). There were no significant differences in the population of the satellite cells between the two groups. The population of adipogenic precursors in the SSP significantly increased than those in the SSC (0.077 $\pm$ 0.030% in SSC vs. 0.110 $\pm$

0.028% in SSP, $p = 0.039$) (Fig. 9B). The ratio of satellite cells/adipogenic precursors in the SSC was significantly higher than that in the SSP ($p<0.001$) (Fig. 9C).

The Correlation between Adipose Infiltration and Precursors' Ratio

The number of patients of the Goutallier classification is as follows: grade 0; 0, grade 1; 1, grade 2; 3, grade 3; 5 and grade 4; 10 (Table. 1). The ratio of the population of myogenic/adipogenic precursors was chosen as the indication of equivalent value of muscle atrophy or fatty infiltration by MRI. There was positive correlation coefficient ($r^2 = 0.5459$, $p<0.001$) between the precursors' ratio and the fatty infiltration (Fig. 10).

Microarray Analysis of Gene Expression Profiles

Expression of 20 genes was significantly higher (Table 3), and the expression of 18 genes was significantly lower in the SSP group compared with the SSC group among approximately 20,000 genes (Table 4). Myosin related factors, such as MYH2 and MYL1 were significantly higher, and homeobox related factors, such as HOXC4 and HOXC6 were significantly lower in the SSP group compared with the SSC group.

20

GO analysis revealed the activation of extracellular organization including multicellular

process and the suppression of the developmental process in satellite cells from the SSP

group (Table. 5, 6).

Myogenic Potential of Satellite Cells Derived from Atrophic Muscles

The satellite cells obtained from the SSC and SSP muscles showed equivalent

ability of proliferation (Fig. 11). Immunofluorescence images of myoblasts/myotubes

identified by myosin heavy chain (MHC) showed satellite cells from both the SSC and

SSP muscles could differentiate to myoblasts/myotubes (Fig. 12). The number of

MHC-positive cells stained with red by anti-MHC antibody was not significantly

different between the SSP and the SSC groups (Fig. 13A). There was no significant

difference in fusion rate between the SSP and the SSC groups (Fig. 13B).

Discussion

The present study revealed the myogenic differentiation potential of satellite cells sorted from the SSP muscle (atrophic) and the SSC muscle (intact) from the same patients. The fatty infiltration was observed as a whole block staining under multi-photon imaging only in the SSP muscle. The satellite cells from the SSP muscle with fatty infiltration could form myotube and had sufficient potential of myogenesis compared with the SSC muscle.

This is the first report of observing human skeletal muscle tissues using multi-photon imaging. It is now becoming widely utilized as a powerful tool for studying the macromolecular microstructures, such as fibril architectures composed of collagen and elastin[12,51,58]. The most significant advantage of multi-photon imaging is its capability of observing non-fixed, unstained tissue samples as a whole mount or in-vivo imaging[15,40,53]. Collagens can be detected as a second harmonic generation signal[24,32], and elastin produce unique two photon excited signal[33], which indicate both fibers can be differentiated without exogenous labels by multi-photon imaging[10]. By taking advantage of the long wave length beam of multi-photon imaging to visualize the deep tissue with 3D microstructure[63], pathophysiological architecture of diseased

muscle tissues observed in rotator cuff tears, such as intramuscular fatty infiltration

surrounded by twisted collagen fibers and meshed blood vessels, can be easily

reconstructed. Recently, Uezumi et al. reported mesenchymal progenitors distinct from

satellite cells contributed to ectopic fat cell formation in skeletal muscles[56]. These

results may indicate that the fatty infiltration of muscle is caused by fat deposition

differentiated from adipogenic precursors rather than fatty degeneration of muscle

fiber. By combining other histochemical staining methods, it would be of great interest

to further identify the mechanism underlying the recruitment of adipogenic precursors

as well as the onset/progress of intramuscular fatty infiltration in pathophysiology of

rotator cuff tears.

The key findings of this study are that human adipogenic progenitors increased

in the atrophic muscle tissues with fatty infiltration, and their population positively

correlates with the severity of fatty infiltration. Although the fatty infiltration is

regarded as a major criterion of the severity of the rotator cuff tears, the population of

the adipogenic progenitors has not been investigated in the atrophic muscle of the

human shoulder. The reason is that the specific adipogenic cell marker had not been

proven. Cells with adipogenic potential have been isolated from human muscle using

CD34 or CD15[35,47,48]. However, both markers are expressed on many different cell types, including myeloid cells of hematopoietic lineage[55]. Uezumi et al. recently reported PDGFRα as a specific marker of human adipogenic progenitors[55]. It enabled me to analyze the population of the mesenchymal stem cells of human muscle. My data strongly suggests that disuse muscle atrophy in rotator cuff tears results in aberrant fatty infiltration along with accumulation of significantly higher numbers of adipogenic precursors in the atrophic regions. In order to examine the pathological relevance of adipogenic precursors, I sorted them from the small amount of human rotator cuff muscles, but did not go well in culture. In a previous report, the culture of adipogenic precursors was conducted by using a large amount of diseased skeletal muscle tissues and by co-culture with digested human muscle cells until reaching the confluence[55]. I chose the direct sorting from digested skeletal muscle cells because the population of satellite cells and adipogenic precursors should be close to initial condition. As a result, I could reveal the significant accumulation of adipogenic precursors in human rotator cuff muscles in relative to the fatty infiltration.

The research about cellular nature of satellite cell is originally developed by using mouse muscle[52,6]. The satellite cell is defined by its location between the basal

lamina and sarcolemma of skeletal muscle fibers[64]. It was identified first in adult frog

skeletal muscle and was subsequently found in other vertebrates including human[6]. The

satellite cell is normally quiescent in adult muscle. They become activated when muscle

is injured and proliferate to generate a pool of muscle precursor cells or myoblasts[64].

Abilities of muscle repair and regeneration in satellite cells are interesting, which is

particularly relevant to the treatment of inherited muscle diseases such as muscular

dystrophy. However, researches about quiescent satellite cells is difficult. In the early

studies, satellite cells were identified by electoron microscopy on the basis of their

position between the basal lamina and sarcolemma of muscle fibers, but this method is

technically demanding and not suitable to large portions of muscle[6]. Their scarcity and

location under the basal lamina of muscle fibers make them difficult to isolate[38]. The

majority of mouse satellite cells can be defined by their expression of Pax7, CD34,

caveolin, calcitonin receptor, beta1-integrin, M-cadherin, alpha7-integrin, and

nestin[6,30,19]. Although markers of human satellite cells are unclear, several studies

reported the identification of satellite cells in human muscles[4,55,59]. M-cadherin and

Pax7 are reliable markers for mouse muscle satellite cells and are also used for human

satellite cell identification[18]. Sca-1 is widely used as a negative selection marker in

mouse[52,38]. However, this antigen, encoded by the mouse gene Ly6a, is not encoded by

the human genome and thus it was not included in our negative selection cocktail[4].

Although CD56 is not expressed by quiescent satellite cells and begins to be expressed

only after denervation or differentiation in mouse[27], both quiescent and activated human

muscle satellite cells express CD56[48]. Therefore, this molecule has been extensively

used as a marker for identification and isolation of satellite cells from human

muscle[55,59].

I took an advantage of FACS technique to sort human satellite cells from both

intace (SSC) and atrophied (SSP) muscle tissues in the same joint and examined their

myogenic potentials. Based upon my compelling data presented in Figs. 8-12, I could

conclude that the satellite cells in atrophic fatty muscles remained largely intact in terms

of both their residential population and myogenic capabilities when compared to those

from healthy region. Considering the fact that fatty infiltration in rotator cuff muscles

could be remained after surgical repair,[20,42] their severities in chronic rotator cuff tears

are recognized as predictors for poor postoperative outcomes[16,34]. Therefore, previous

study has focused on regenerative capability of satellite cells in rotator cuff muscles as a

central role of healing process[37]. It has been difficult to sort human satellite cells from

muscles because the number of satellite cells sorted from FACS is very small[4]. Bareja et

al. used approximately 2-3g of the gracilis and sartorius muscles discarded when anterior cruciate ligament reconstruction surgery was conducted[4]. Uezumi et al. used co-cultured muscles of rectus femoris or biceps brachii of Duchenne muscular dystrophy patients[55]. I have succeeded in direct sorting from small amount of human muscles (approximately 0.3 g), which enabled me to analyze the myogenic potential of satellite cells in normal and atrophic muscles of the same patient. Meyer et al. recently compared myogenic potentials of muscle progenitor cells among 3 groups; bursitis, partial thickness rotator cuff tears, and full thickness rotator cuff tears[37]. Although they did not sort human satellite cells using FACS, they indicated no significant difference about the muscle regenerative capacities among the 3 groups. My data also supports their results that the satellite cells even from the fatty atrophic muscles can form the myotube. Despite rapid improvements in surgical techniques and instrumentation, the healing failure rate after surgical repair is considerably high[22]. The effects of repair on fatty infiltration remain controversial[29,42,43]. My result indicated the clinical benefits of recovery of atrophic muscle after rotator cuff repair surgery even though the fatty infiltration existed. The prevention for the accumulating adipogenic precursors may be a therapeutic target for the recovery from severe rotator cuff tears.

The DNA microarray analysis of the satellite cells indicated several representative tendencies including greater myogenesis in the SSP, such as MYH2, MYH8, MYL1, and COL6A6. Choo et al. reported that muscle gene expression patterns varied according to tendon injury severities in human rotator cuff tears[11]. It should be noted that my paired samples, taken from the same shoulder joint, excluded differences of the genetic background. Taken together with the poor improvement after severe rotator cuff tears, I assume that the fatty infiltration and loss of mechanical stress in rotator cuff muscles wouldn't affect the myogenic ability of satellite cells, but they lead to change niche construction, such as the increase of adipogenic cells[7,26,62]. The changes of niche construction including the adipogenic cells may have some roles of inhibiting the myotube fiber synthesis although the satellite cells from SSP muscle express higher myogenic tendencies compared to the ones from the SSC[7,28,44].

The limitations of this study were that the definition of the myogenic precursor cells has a possibility of including neuronal cells in FACS, the SSC muscle was defined as healthy muscle in a pathologic joint, there may be fundamental differences between the two muscles, the accuracy of the MRI study, and the differentiation of the adipogenic precursor. The satellite cells were defined as CD56 positive cells, and the

heamatopoietic cells were excluded by CD45, CD11b, and CD31. Because the marker

of the neuronal cells has not been defined precisely, there may be contamination of

neuronal cells in this set. Although I defined the SSP muscle as a control of healthy

muscle, strictly speaking, the SSP is not a healthy muscle because it is in a pathologic

joint of rotator cuff tear. There are some functional differences between the SSP and

SSC.   The SSP mainly plays a role of upper elevation, while the SSC plays a role of

humeral rotation. The muscle atrophy was evaluated by MRI with 3 series of Y-view

images, however, this could not reflect the precise muscle volume and fatty infiltration.

After the rotator cuff tear, the muscle was retracted and the tear size assumes to be

greater with the Y-view image. The 3D MRI of the whole muscle should be evaluated.

The differentiation of the adipogenic precursor was not observed in culture although the

population was correlated with the severity of muscle atrophy. The proper handling of

the antibody or adipogenic culture should be needed.

Because getting the myogenic precursor cells from small quantity of the human

muscles, I have a plan to establish in vitro exercise model, which can conduct electric

stimuli under culture condition. This system can evaluate factors related contraction of

muscles, such as myokine, which leads to the cure of the diabetes and be able to analyze

the responsible genes of the muscle disease of sarcopenia, muscle dystrophies, and

sporadic inclusion body myositis.

Conclusions

The present study suggested as follows: (1) The adipogenic deposition near the blood vessels was observed in the human muscle with fatty infiltration as a whole block staining under multi-photon imaging, (2) The satellite cells could be sorted from atrophic and intact muscles from the same patients, (3) The satellite cells from atrophic muscles with fatty infiltration could form myotube and had sufficient potential of myogenesis compared to the intact muscles, (4) The satellite cell in the atrophic muscles kept myogenic tendency by DNA microarray, (5) The adipogenic progenitors increased in the atrophic muscles, (6) The ratio of the population of adipogenic progenitors and satellite cells correlated with the severity of fatty infiltration evaluated by MRI.

The human satellite cells even from the atrophic muscles with fatty infiltration of rotator cuff tears could maintain the intrinsic myogenic potentials, while the accumulation of adipogenic precursors is distinct in human atrophic muscles. The proper handling/prevention for the accumulating adipogenic precursors may be a therapeutic target for the recovery from severe rotator cuff tears. My result indicated the clinical benefits of recovery of atrophic muscle after rotator cuff repair surgery even though the fatty infiltration existed.

References

1.   Aas V, Bakke SS, Feng YZ, et al. Are cultured human myotubes far from home? *Cell Tissue Res*. 2013;354(3):671-682. doi:10.1007/s00441-013-1655-1.

2.   Ariga M, Nedachi T, Katagiri H, Kanzaki M. Functional role of sortilin in myogenesis and development of insulin-responsive glucose transport system in C2C12 myocytes. *J Biol Chem*. 2008;283(15):10208-10220. doi:10.1074/jbc.M710604200.

3.   Asakura A. Skeletal Muscle-derived Hematopoietic Stem Cells: Muscular Dystrophy Therapy by Bone Marrow Transplantation. *J Stem Cell Res Ther*. 2012;Suppl 11. doi:10.4172/2157-7633.S11-005.

4.   Bareja A, Holt J a, Luo G, et al. Human and mouse skeletal muscle stem cells: convergent and divergent mechanisms of myogenesis. *PLoS One*. 2014;9(2):e90398. doi:10.1371/journal.pone.0090398.

5.   Barry JJ, Lansdown D a, Cheung S, Feeley BT, Ma CB. The relationship between tear severity, fatty infiltration, and muscle atrophy in the supraspinatus. *J Shoulder Elbow Surg*. 2013;22(1):18-25. doi:10.1016/j.jse.2011.12.014.

6. Boldrin L, Muntoni F, Morgan JE. Are human and mouse satellite cells really the same? *J Histochem Cytochem*. 2010;58(11):941-955. doi:10.1369/jhc.2010.956201.

7. Boppart MD, De Lisio M, Zou K, Huntsman HD. Defining a role for non-satellite stem cells in the regulation of muscle repair following exercise. *Front Physiol*. 2013;4(November):310. doi:10.3389/fphys.2013.00310.

8. Buch A, Carmeli E, Boker LK, et al. Muscle function and fat content in relation to sarcopenia, obesity and frailty of old age — An overview. *Exp Gerontol*. 2016;76:25-32. doi:10.1016/j.exger.2016.01.008.

9. Castiglioni A, Hettmer S, Lynes MD, et al. Isolation of Progenitors that Exhibit Myogenic/Osteogenic Bipotency In Vitro by Fluorescence-Activated Cell Sorting from Human Fetal Muscle. *Stem cell reports*. 2014;2(1):92-106. doi:10.1016/j.stemcr.2013.12.006.

10. Chen J, Zhuo S, Jiang X, et al. Multiphoton microscopy study of the morphological and quantity changes of collagen and elastic fiber components in keloid disease. *J Biomed Opt*. 2011;16(5):51305. doi:10.1117/1.3569617.

11.   Choo A, Mccarthy M, Pichika R, et al. Muscle Gene Expression Patterns in.

       2014:1558-1565.

12.   Cui JZ, Tehrani AY, Jett K a., Bernatchez P, van Breemen C, Esfandiarei M.

       Quantification of aortic and cutaneous elastin and collagen morphology in

       Marfan syndrome by multiphoton microscopy. *J Struct Biol*.

       2014;187(3):242-253. doi:10.1016/j.jsb.2014.07.003.

13.   DePalma AF. The classic. Surgical anatomy of the rotator cuff and the natural

       history of degenerative periarthritis. Surg Clin North Am. 1963;43:1507-1520.

       Clin Orthop Relat Res. 2008;466(3):543-551. doi:10.1007/s11999-007-0103-5.

14.   Deprés-tremblay G, Chevrier A, Snow M, Hurtig MB, Rodeo S, Buschmann MD.

       Rotator cuff repair: a review of surgical techniques, animal models, and new

       technologies under development. *J Shoulder Elb Surg*. 2016.

       doi:10.1016/j.jse.2016.06.009.

15.   Egawa G, Miyachi Y, Kabashima K. Identification of perivascular adipose tissue

       in the mouse skin using two-photon microscopy. *J Dermatol Sci*.

       2013;70(2):139-140. doi:10.1016/j.jdermsci.2013.02.009.

16. Fermont AJM, Wolterbeek N, Wessel RN, Baeyens J-P, de Bie R a. Prognostic factors for successful recovery after arthroscopic rotator cuff repair: a systematic literature review. *J Orthop Sports Phys Ther*. 2014;44(3):153-163. doi:10.2519/jospt.2014.4832.

17. Fuchs B, Weishaupt D, Zanetti M, Hodler J, Gerber C. Fatty degeneration of the muscles of the rotator cuff: assessment by computed tomography versus magnetic resonance imaging. *J Shoulder Elbow Surg*. 8(6):599-605. http://www.ncbi.nlm.nih.gov/pubmed/10633896. Accessed December 22, 2015.

18. Fukada S, Higuchi S, Segawa M, et al. Purification and cell-surface marker characterization of quiescent satellite cells from murine skeletal muscle by a novel monoclonal antibody. *Exp Cell Res*. 2004;296(2):245-255. doi:10.1016/j.yexcr.2004.02.018.

19. Fukada S-I, Ma Y, Ohtani T, Watanabe Y, Murakami S, Yamaguchi M. Isolation, characterization, and molecular regulation of muscle stem cells. *Front Physiol*. 2013;4(November):317. doi:10.3389/fphys.2013.00317.

20. Gladstone JN, Bishop JY, Lo IKY, Flatow EL. Fatty infiltration and atrophy of the rotator cuff do not improve after rotator cuff repair and correlate with poor functional outcome. *Am J Sports Med*. 2007;35(5):719-728. doi:10.1177/0363546506297539.

21. Goutallier D, Postel JM, Bernageau J, Lavau L, Voisin MC. Fatty muscle degeneration in cuff ruptures. Pre- and postoperative evaluation by CT scan. *Clin Orthop Relat Res*. 1994;(304):78-83. http://www.ncbi.nlm.nih.gov/pubmed/8020238. Accessed December 22, 2015.

22. Goutallier D, Postel J-M, Gleyze P, Leguilloux P, Van Driessche S. Influence of cuff muscle fatty degeneration on anatomic and functional outcomes after simple suture of full-thickness tears. *J Shoulder Elbow Surg*. 12(6):550-554. doi:10.1016/S1058274603002118.

23. Hagiwara Y, Ando A, Onoda Y, et al. Coexistence of fibrotic and chondrogenic process in the capsule of idiopathic frozen shoulders. *Osteoarthr Cartil*. 2012. doi:10.1016/j.joca.2011.12.008.

24. Huang Z, Zhuo S, Chen J, Chen R, Jiang X. Multiphoton microscopic imaging of adipose tissue based on second-harmonic generation and two-photon excited fluorescence. *Scanning*. 2008;30(August):452-456. doi:10.1002/sca.20130.

25. Hunt LC, Demontis F. Whole-mount immunostaining of Drosophila skeletal muscle. *Nat Protoc*. 2013;8(12):2496-2501. doi:10.1038/nprot.2013.156.

26. Imaoka Y, Kawai M, Mori F, Miyata H. Effect of eccentric contraction on satellite cell activation in human vastus lateralis muscle. *J Physiol Sci*. 2015. doi:10.1007/s12576-015-0385-4.

27. Irintchev A, Zeschnigk M, Starzinski-Powitz A, Wernig A. Expression pattern of M-cadherin in normal, denervated, and regenerating mouse muscles. *Dev Dyn*. 1994;199(4):326-337. doi:10.1002/aja.1001990407.

28. Joe AWB, Yi L, Natarajan A, et al. Muscle injury activates resident fibro/adipogenic progenitors that facilitate myogenesis. *Nat Cell Biol*. 2010;12(2):153-163. doi:10.1038/ncb2015.

29.   Jost B, Zumstein M, Pfirrmann CW a, Gerber C. Long-term outcome after

       structural failure of rotator cuff repairs. *J Bone Joint Surg Am.*

       2006;88(3):472-479. doi:10.2106/JBJS.E.00003.

30.   Judson RN, Zhang R-H, Rossi FM a. Tissue-resident mesenchymal

       stem/progenitor cells in skeletal muscle: collaborators or saboteurs? *FEBS J.*

       2013;280(17):4100-4108. doi:10.1111/febs.12370.

31.   Killian ML, Cavinatto LM, Ward SR, Havlioglu N, Thomopoulos S, Galatz LM.

       Chronic Degeneration Leads to Poor Healing of Repaired Massive Rotator Cuff

       Tears in Rats. *Am J Sports Med*. 2015. doi:10.1177/0363546515596408.

32.   Kottmann RM, Sharp J, Owens K, et al. Second harmonic generation microscopy

       reveals altered collagen microstructure in usual interstitial pneumonia versus

       healthy lung. *Respir Res*. 2015;16(1):1-13. doi:10.1186/s12931-015-0220-8.

33.   Kwon GP, Schroeder JL, Amar MJ, Remaley AT, Balaban RS. Contribution of

       macromolecular structure to the retention of low-density lipoprotein at arterial

       branch points. *Circulation*. 2008;117(22):2919-2927.

       doi:10.1161/CIRCULATIONAHA.107.754614.

34.   Laron D, Samagh SP, Liu X, Kim HT, Feeley BT. Muscle degeneration in rotator

        cuff tears. *J Shoulder Elbow Surg*. 2012;21(2):164-174.

        doi:10.1016/j.jse.2011.09.027.

35.   Lecourt S, Marolleau J-P, Fromigué O, et al. Characterization of distinct

        mesenchymal-like cell populations from human skeletal muscle in situ and in

        vitro. *Exp Cell Res*. 2010;316(15):2513-2526. doi:10.1016/j.yexcr.2010.04.020.

36.   Liem D, Lichtenberg S, Magosch P, Habermeyer P. Magnetic resonance imaging

        of arthroscopic supraspinatus tendon repair. *J Bone Joint Surg Am*.

        2007;89(8):1770-1776. doi:10.2106/JBJS.F.00749.

37.   Meyer G a., Farris AL, Sato E, et al. Muscle progenitor cell regenerative capacity

        in the torn rotator cuff. *J Orthop Res*. 2015;(March):n/a-n/a.

        doi:10.1002/jor.22786.

38.   Montarras D, Morgan J, Collins C, et al. Direct isolation of satellite cells for

        skeletal muscle regeneration. *Science*. 2005;309(5743):2064-2067.

        doi:10.1126/science.1114758.

39. Müller H, Schmidt D, Dreher F, Herwig R, Ploubidou A, Lange BM. Gene

ontology analysis of the centrosome proteomes of Drosophila and human.

Commun Integr Biol. 2011;4(3):308-311. doi:10.4161/cib.4.3.14806.

40. Nishimura S, Manabe I, Nagasaki M, et al. In vivo imaging in mice reveals local

cell dynamics and inflammation in obese adipose tissue. 2008;118(2).

doi:10.1172/JCI33328DS1.

41. Nishimura S, Manabe I, Nagasaki M, et al. In vivo imaging visualizes discoid

platelet aggregations without endothelium disruption and implicates contribution

of inflammatory cytokine and integrin signaling. *Blood*. 2012;119(8):45-57.

doi:10.1182/blood-2011-09-381400.

42. Oh JH, Chung SW, Kim SH, Chung JY, Kim JY. 2013 Neer Award: Effect of the

adipose-derived stem cell for the improvement of fatty degeneration and rotator

cuff healing in rabbit model. *J Shoulder Elbow Surg*. 2014;23(4):445-455.

doi:10.1016/j.jse.2013.07.054.

43. Osti L, Buda M, Buono A Del. Fatty infiltration of the shoulder : diagnosis and

reversibility Corresponding author : 2013:351-354.

44. Penton CM, Thomas-Ahner JM, Johnson EK, McAllister C, Montanaro F. Muscle Side Population Cells from Dystrophic or Injured Muscle Adopt a Fibro-Adipogenic Fate. *PLoS One*. 2013;8(1). doi:10.1371/journal.pone.0054553.

45. Perruchot M-H, Lefaucheur L, Barreau C, Casteilla L, Louveau I. Age-related changes in the features of porcine adult stem cells isolated from adipose tissue and skeletal muscle. *Am J Physiol Cell Physiol*. 2013;305(7):C728-38. doi:10.1152/ajpcell.00151.2013.

46. Pisani DF, Bottema CDK, Butori C, Dani C, Dechesne C a. Mouse model of skeletal muscle adiposity: a glycerol treatment approach. *Biochem Biophys Res Commun*. 2010;396(3):767-773. doi:10.1016/j.bbrc.2010.05.021.

47. Pisani DF, Clement N, Loubat A, et al. Hierarchization of myogenic and adipogenic progenitors within human skeletal muscle. *Stem Cells*. 2010;28:2182-2194. doi:10.1002/stem.537.

48.   Pisani DF, Dechesne C a, Sacconi S, et al. Isolation of a highly myogenic

CD34-negative subset of human skeletal muscle cells free of adipogenic potential.

Stem Cells. 2010;28(4):753-764. doi:10.1002/stem.317.

49.   Rothstein EC, Nauman M, Chesnick S, Balaban RS. Multi-photon excitation

microscopy in intact animals. *J Microsc*. 2006;222(1):58-64.

doi:10.1111/j.1365-2818.2006.01570.x.

50.   Sanada K, Miyachi M, Tanimoto M, et al. A cross-sectional study of sarcopenia

in Japanese men and women: reference values and association with

cardiovascular risk factors. *Eur J Appl Physiol*. 2010;110(1):57-65.

doi:10.1007/s00421-010-1473-z.

51.   Schenke-Layland K, Riemann I, Damour O, Stock U a., König K. Two-photon

microscopes and in vivo multiphoton tomographs - Powerful diagnostic tools for

tissue engineering and drug delivery. *Adv Drug Deliv Rev*. 2006;58(7):878-896.

doi:10.1016/j.addr.2006.07.004.

52.   Sherwood RI, Christensen JL, Conboy IM, et al. Isolation of adult mouse

       myogenic progenitors: functional heterogeneity of cells within and engrafting

       skeletal muscle. *Cell*. 2004;119(4):543-554. doi:10.1016/j.cell.2004.10.021.

53.   Tang P, Zhang Y, Chen C, et al. In Vivo Two-Photon Imaging of Axonal

       Dieback, Blood Flow, and Calcium Influx with Methylprednisolone Therapy

       after Spinal Cord Injury. *Sci Rep*. 2015;5:9691. doi:10.1038/srep09691.

54.   Tempelhof S, Rupp S, Seil R. Age-related prevalence of rotator cuff tears in

       asymptomatic shoulders. *J Shoulder Elbow Surg*. 8(4):296-299.

       http://www.ncbi.nlm.nih.gov/pubmed/10471998. Accessed December 22, 2015.

55.   Uezumi   a, Fukada S, Yamamoto N, et al. Identification and characterization of

       PDGFRα+ mesenchymal progenitors in human skeletal muscle. *Cell Death Dis*.

       2014;5:e1186. doi:10.1038/cddis.2014.161.

56.   Uezumi A, Fukada S, Yamamoto N, Takeda S, Tsuchida K. Mesenchymal

       progenitors distinct from satellite cells contribute to ectopic fat cell formation in

       skeletal muscle. *Nat Cell Biol*. 2010;12(2):143-152. doi:10.1038/ncb2014.

57.   Walston JD. Sarcopenia in older adults. *Curr Opin Rheumatol*.

        2012;24(6):623-627. doi:10.1097/BOR.0b013e328358d59b.

58.   Wang BG, König K, Halbhuber KJ. Two-photon microscopy of deep intravital

        tissues and its merits in clinical research. *J Microsc*. 2010;238(1):1-20.

        doi:10.1111/j.1365-2818.2009.03330.x.

59.   Xu X, Wilschut KJ, Kouklis G, et al. Human Satellite Cell Transplantation and

        Regeneration from Diverse Skeletal Muscles. *Stem Cell Reports*.

        2015;5(3):419-434. doi:10.1016/j.stemcr.2015.07.016.

60.   Yabe Y, Hagiwara Y, Ando A, et al. Chondrogenic and fibrotic process in the

        ligamentum flavum of patients with lumbar spinal canal stenosis. *Spine (Phila Pa

        1976)*. 2015;40(7):429-435. doi:10.1097/BRS.0000000000000795.

61.   Yabe Y, Hagiwara Y, Ando A, et al. Chondrogenic and fibrotic process in the

        ligamentum flavum of patients with lumbar spinal canal stenosis. *Spine (Phila Pa

        1976)*. 2015;40(7):429-435. doi:10.1097/BRS.0000000000000795.

62.   Yin H, Price F, Rudnicki M a. Satellite cells and the muscle stem cell niche.

        Physiol Rev. 2013;93(1):23-67. doi:10.1152/physrev.00043.2011.

63. Zadrozny LM, Neufeld EB, Lucotte BM, et al. Study of the Development of the Mouse Thoracic Aorta Three-Dimensional Macromolecular Structure using Two-Photon Microscopy. *J Histochem Cytochem*. 2014;63(1):8-21. doi:10.1369/0022155414559590.

64. Zammit PS, Partridge T a, Yablonka-Reuveni Z. The skeletal muscle satellite cell: the stem cell that came in from the cold. *J Histochem Cytochem*. 2006;54(11):1177-1191. doi:10.1369/jhc.6R6995.2006.

Figure Legends

Fig. 1: Scheme of antero-posterior view of the right shoulder joint and sampling procedure

The shoulder is made up of three bones; the humerus, scapula, and clavicle. The shoulder is a ball-and-socket joint and the humeral head is kept in the shoulder socket by the rotator cuff. The rotator cuff is a network of four muscles (SSC, SSP, infraspinatus, and teres minor muscl muscle) that come together as tendons to form a covering around the head of the humerus. The subscapularis covers the front of the scapula, and the supraspinatus covers upper of the scapula. Both infraspinatus and teres minor muscles cover the back of the scapula. The rotator cuff attaches the humerus to the shoulder blade and helps to lift and rotate the arm. Muscle biopsies (approximately 300 mg) were obtained from the middle of the SSP and SSC muscles from the same joint, respectively. This figure was created with Anatomography. http://lifesciencedb.jp/bp3d

Fig. 2: Goutallier classification of muscle atrophy and fatty infiltration

Grade 0: normal, Grade 1: some fat streaks, Grade 2: fatty degeneration of less than 50%, Grade 3: 50% fatty muscle atrophy; and Grade 4: fatty infiltration of more than 50%.

Fig. 3: Evaluation of muscle atrophy with magnetic resonance imaging conducted before surgery

A: Lateral aspect of the left shoulder

B: Sagittal view of magnetic resonance imaging

The muscle atrophy was calculated based on Goutalier protocol on MRI conducted before the operation. This protocol was used to analyze the most lateral sagittal-oblique image where the acromion, coracoid, and scapular body were all visible, together with the next 2 consecutive lateral images. The sagittal-oblique image of the scapula was viewed from the circle indicated Fig. 1. Muscle atrophy was calculated by the ratio of the area of muscle and fat. The center of Y image shows scapula. Red area: muscle. Yellow area: muscle and fat. Muscle atrophy was calculated as red/yellow area.

Fig. 2A was created with Anatomography. http://lifesciencedb.jp/bp3d

Fig. 4: The multi-photon imaging of the rotator cuff muscles without staining.

A: The muscle fibers of SSC muscle; B: The adipogenic tissue of SSP muscle.

Muscle fibers can be recognized with green auto-fluorescence (A). The adipogenic tissue within the muscle fibers could not be recognized without staining (B). The collagen fibers surrounding the adipogenic tissue could be seen with blue signal.

Fig. 5: The multi-photon imaging of the rotator cuff muscles with staining.

A: SSC; B: SSP

The SSC and SSP muscle samples stained with BODIPY 558/568 C12, Hoechst 33342 and Alexa Fluor 488-conjugated isolectin GS-IB4 were observed. The nuclei of the cells stained with Heachst 33342 with blue signal were scattered around the sarcomere (A). The adipogenic tissue stained with BODIPY could be recognized with multi-photon imaging (B). White arrow: nuclei. White arrow head: adipogenic tissue stained with BODIPY

Fig. 6: Three dimensional reconstruction of the multi-photon imaging of the rotator cuff muscles.

A: SSC; B: SSP

Muscle fibers were excited with green autofluorescence. Compared with the SSC (A), the muscle tissue in the SSP contained fat tissues stained with BODIPY (*: red) surrounded by collagen fibers (blue) (B). White arrow: sarcomeres. White arrow head: capillary vessels.

Fig. 7: Flowcytometry of myogenic precursors from the rotator cuff muscles.

A: SSC; B: SSP.

The dead cells stained with DAPI and doublets were removed by gating strategy. The gate was set by negative control. Each of satellite cells of the SSC and SSP was sorted by FACS. In the SSC muscle, 0.16 % of total events could be sorted (A). In the SSP muscle, 0.10 % of total events could be sorted.

Fig. 8: Flowcytometry of adipogenic precursors from rotator cuff muscles.

A: SSC; B: SSP.

The dead cells stained with DAPI and doublets were removed by gating strategy. The gate was set by negative control. Each of adipogenic precursors of the SSC and SSP was sorted by FACS. In the SSC muscle, 0.038 % of total events could be sorted (A). In the SSP muscle, 0.086 % of total events could be sorted (B).

Fig. 9: The ratio of myogenic and adipogenic precursors from rotator cuff muscles.

A: The population ratio of myogenic precursors in the total events.

B: The population ratio of adipogenic precursors in the total events.

C: The ratio of myogenic/adipogenic precursors

The ratio of satellite cells in the SSC muscle tend to be higher than those in the SSP muscle (A). The ratio of adipogenic precursors in the SSP muscle was significantly higher than those in the SSC muscle ($p = 0.039$) (B). The ratio of satellite cells /

adipogenic precursors was significantly higher in the SSC muscle than the SSP muscle ($p<0.001$) (C). Experimental values are given as the mean ± SEM.
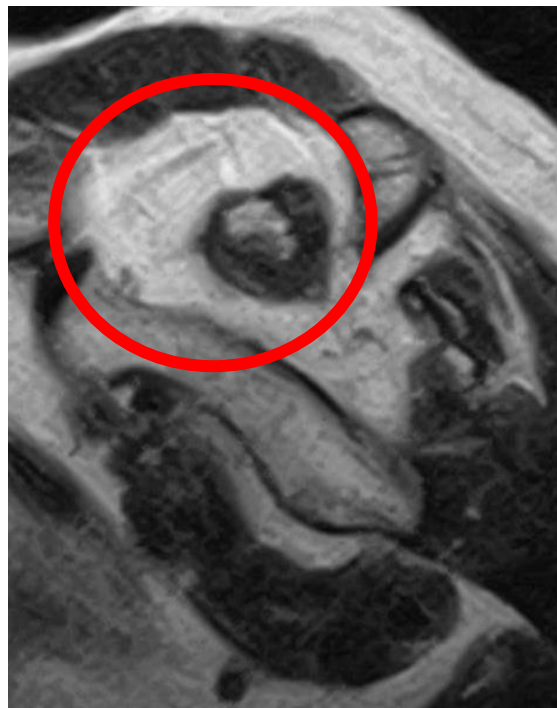
Fig. 10: The correlation between the ratios of the progenitors and a degree of muscle atrophy evaluated by magnetic resonance imaging.

There was positive correlation between the ratio of satellite cells / adipogenic precursors population and the ratio of the muscle atrophy evaluated by magnetic resonance imaging conducted ($p<0.001$).

Fig. 11: The proliferation of cultured satellite cells.

A: SSC; B: SSP

The satellite cells obtained from the SSC and SSP muscles showed equivalent ability of proliferation.

Fig. 12: The myogenic differentiation of the satellite cells.

A: Immunofluorescence images of SSC; B: SSP

Immunofluorescence images of myoblasts/myotubes identified by myosin heavy chain (MHC, red) showed the satellite cells from both the SSC and SSP muscles could differentiate to myoblasts/myotubes.

Fig. 13: The analysis of the myogenic differentiation

A: The number of myosin positive cells of SSC and SSP

B: The fusion rate of SSC and SSP

The number of MHC-positive cells (A) and the fusion rate (B), which is the number of nuclei (Blue) in myotubes (DAPI, blue), were calculated. There was no significant difference between the SSP and SSC muscles. Experimental values are given as the mean ± SEM.
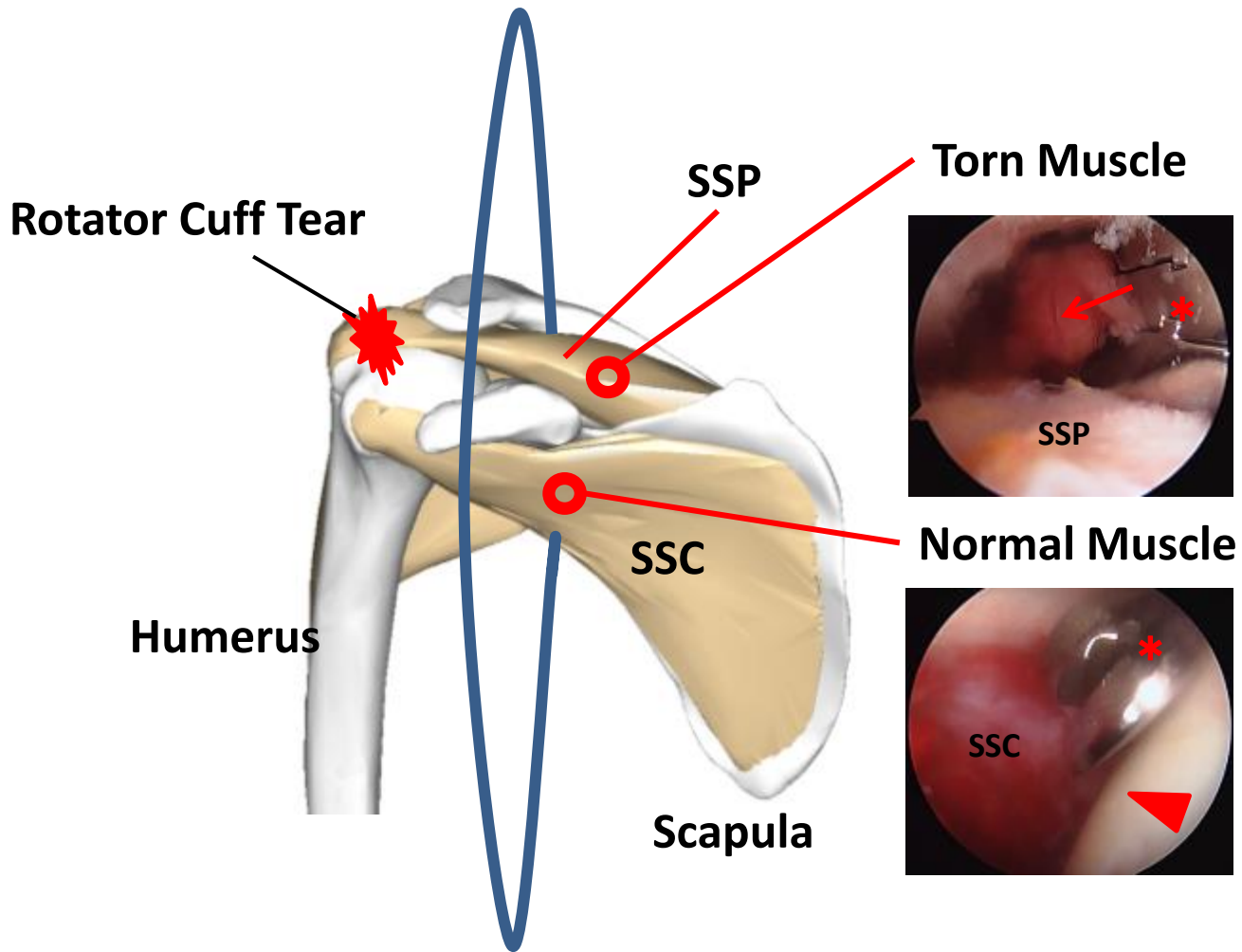
Fig. 1

Fig. 2
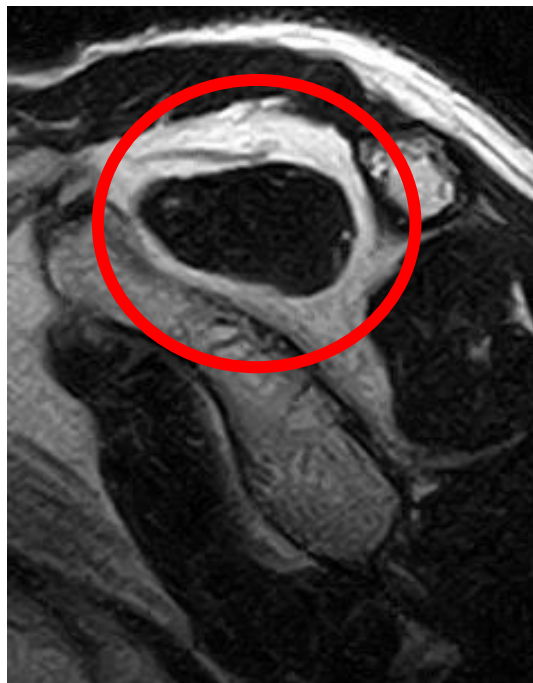
Grade 0

Grade 1
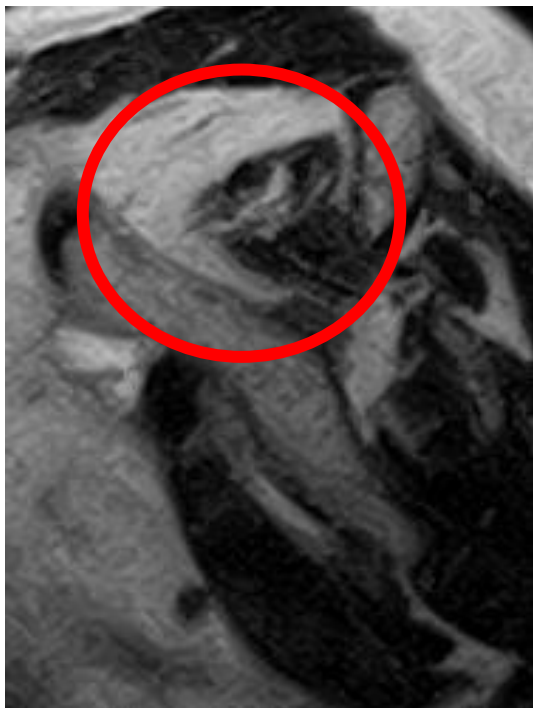
Grade 3

Grade 4

Fig. 3
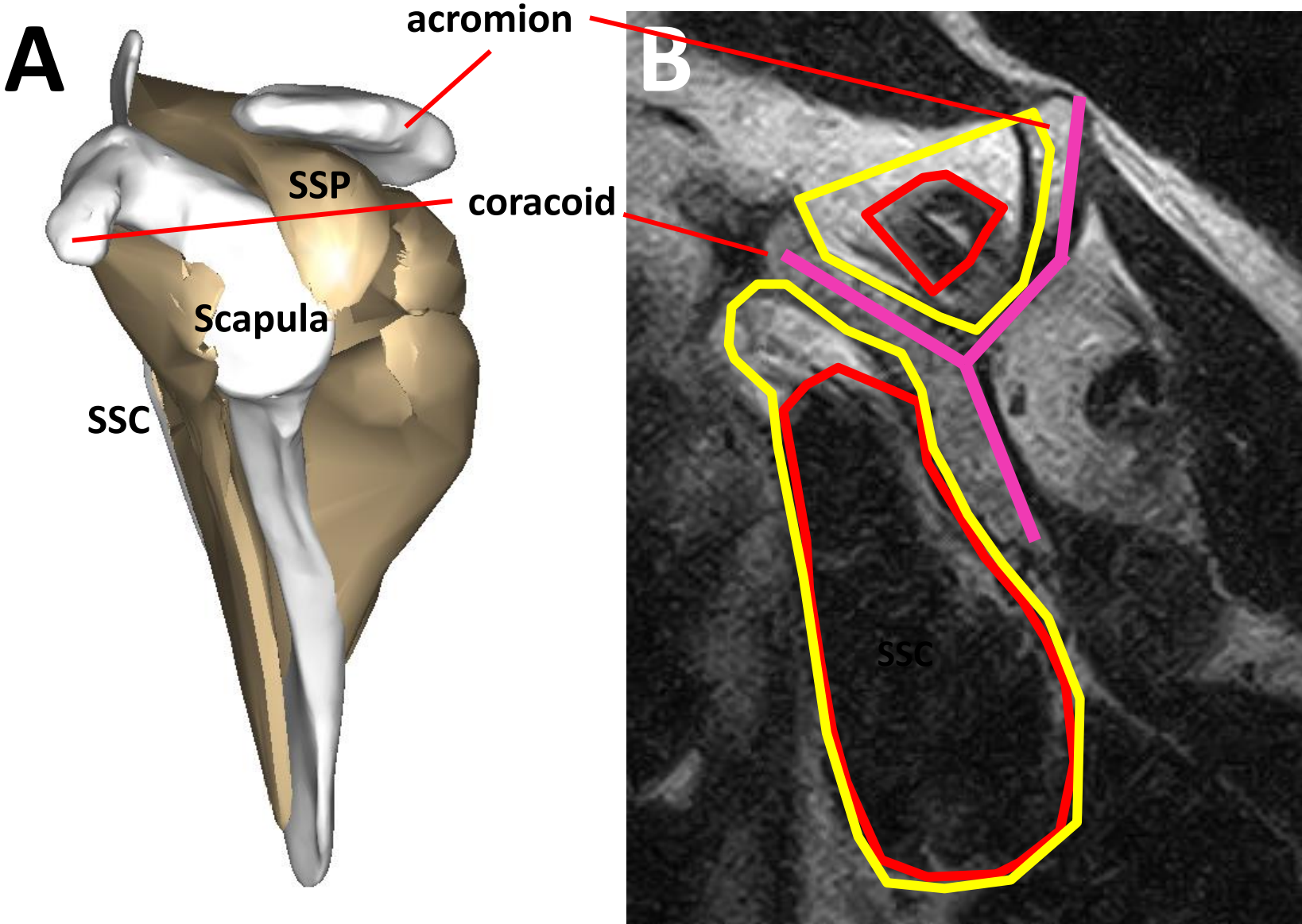
Fig. 4
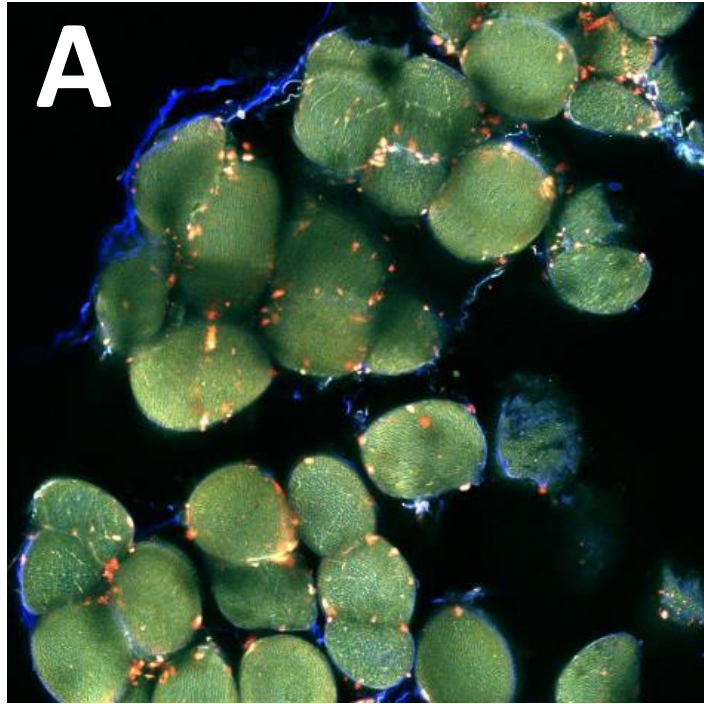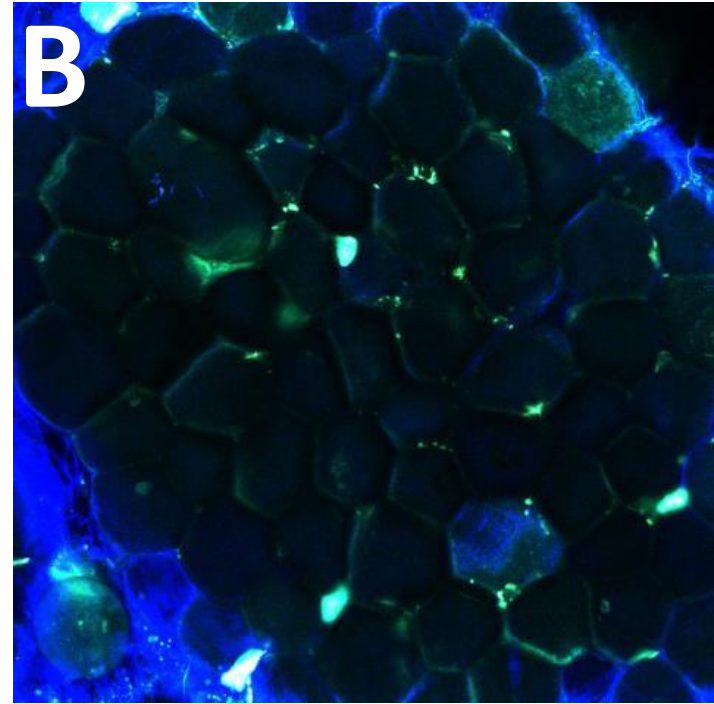
SSC   **SSP**

Fig. 5

SSC   SSP

Fig. 6

A SSC

B SSP

Fig. 7

Fig. 8

Fig. 9

Fig. 10

Scatter plot with x-axis labeled "Myogenic Cell/Adipogenic Cell (FACS)" ranging from 0 to 16, and y-axis labeled "Grading of Muscle Atrophy (MRI)" ranging from 0 to 1.2. A linear trend line is shown with $R^2 = 0.5459$.
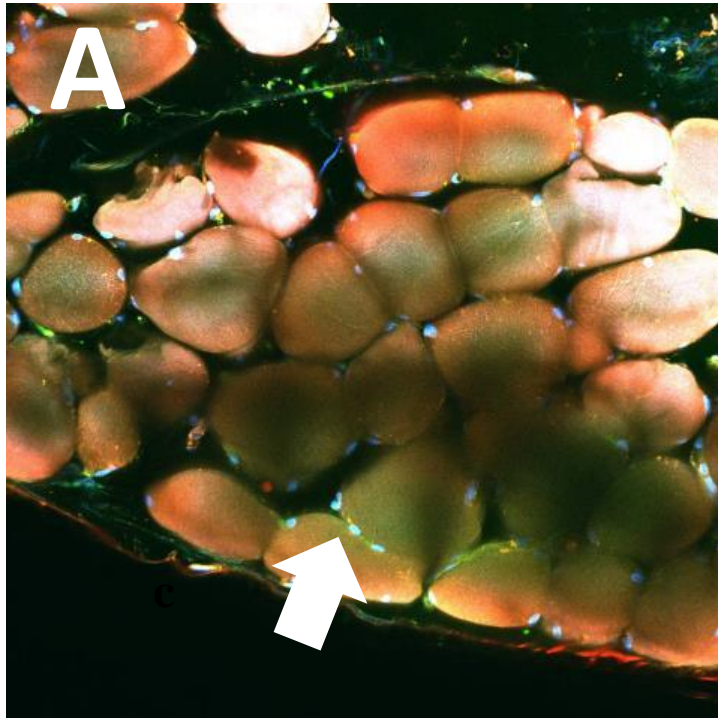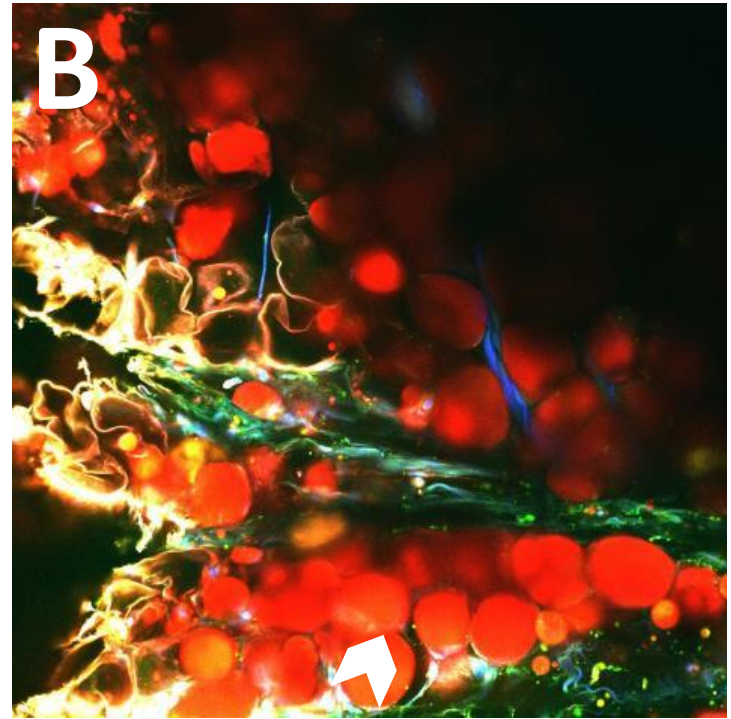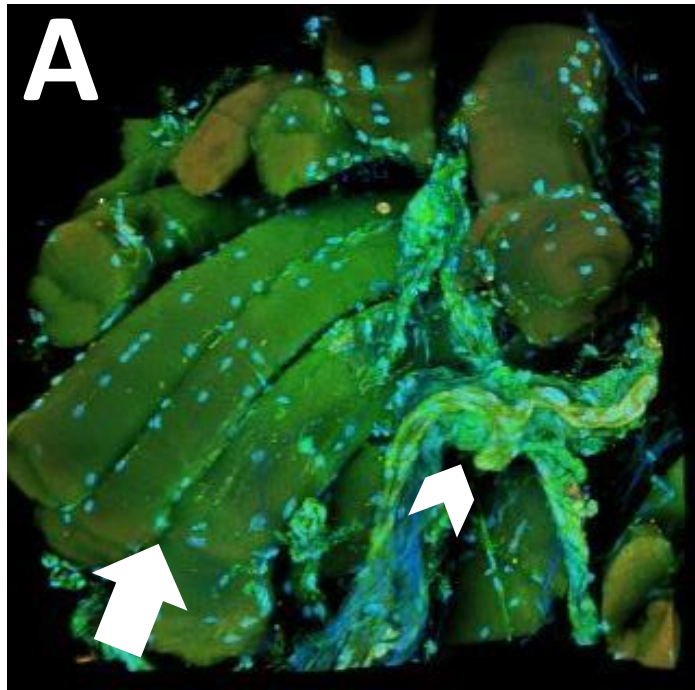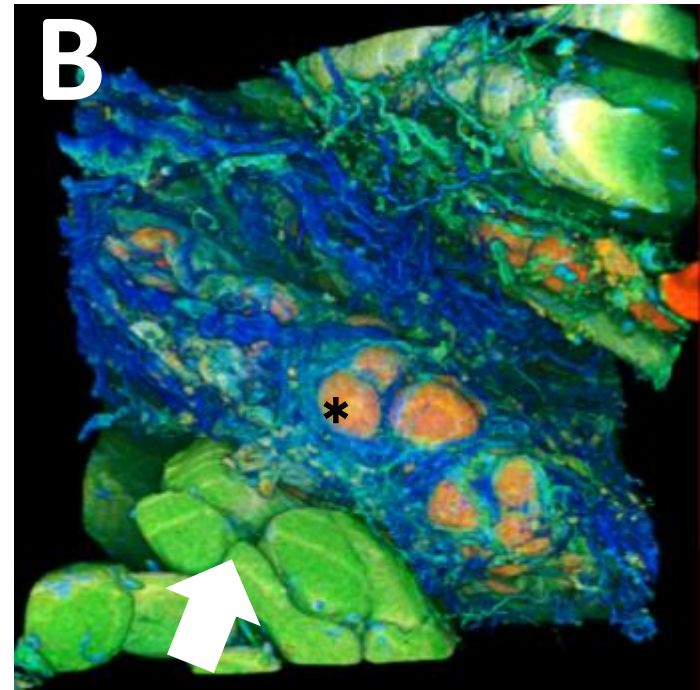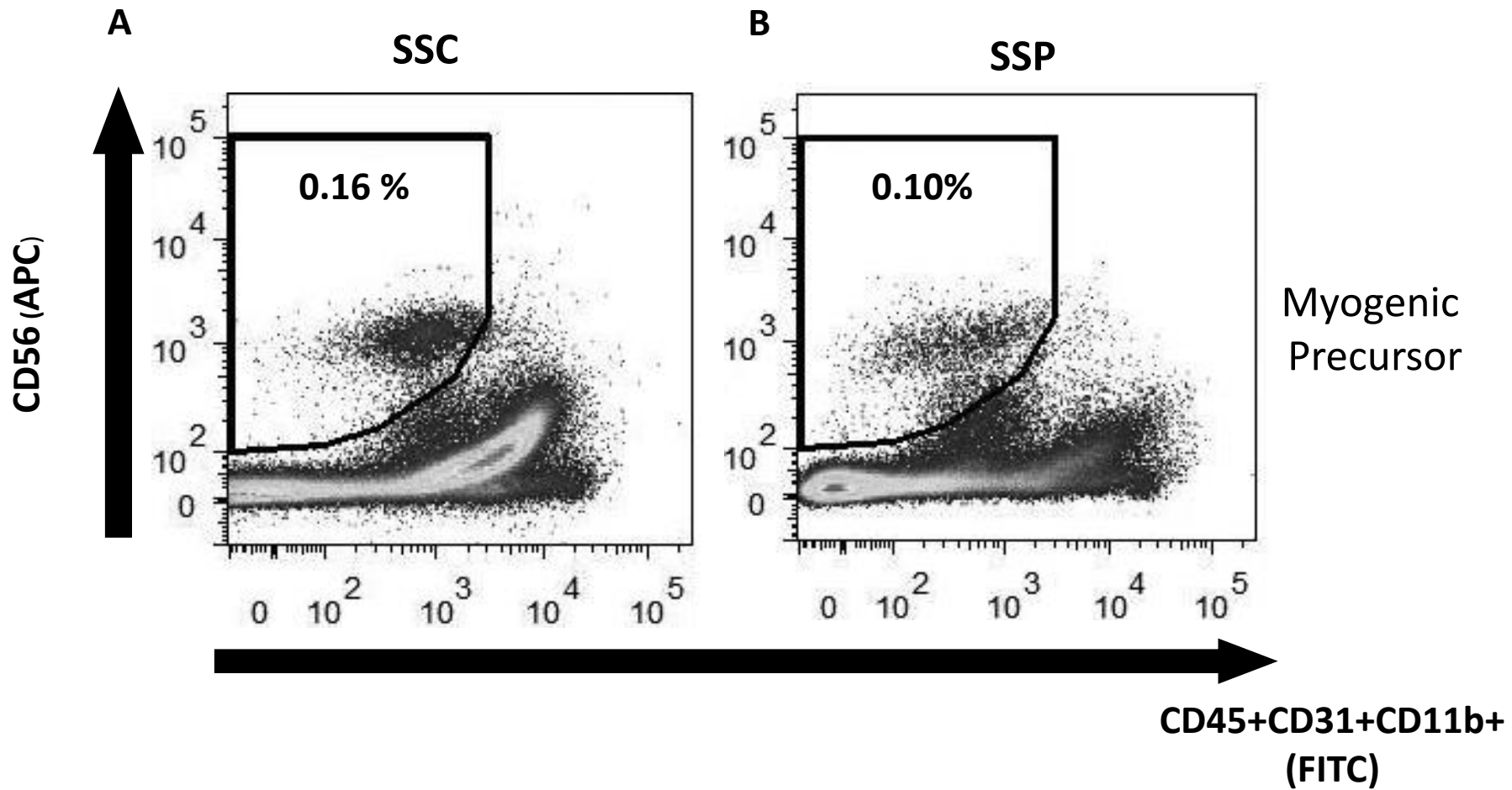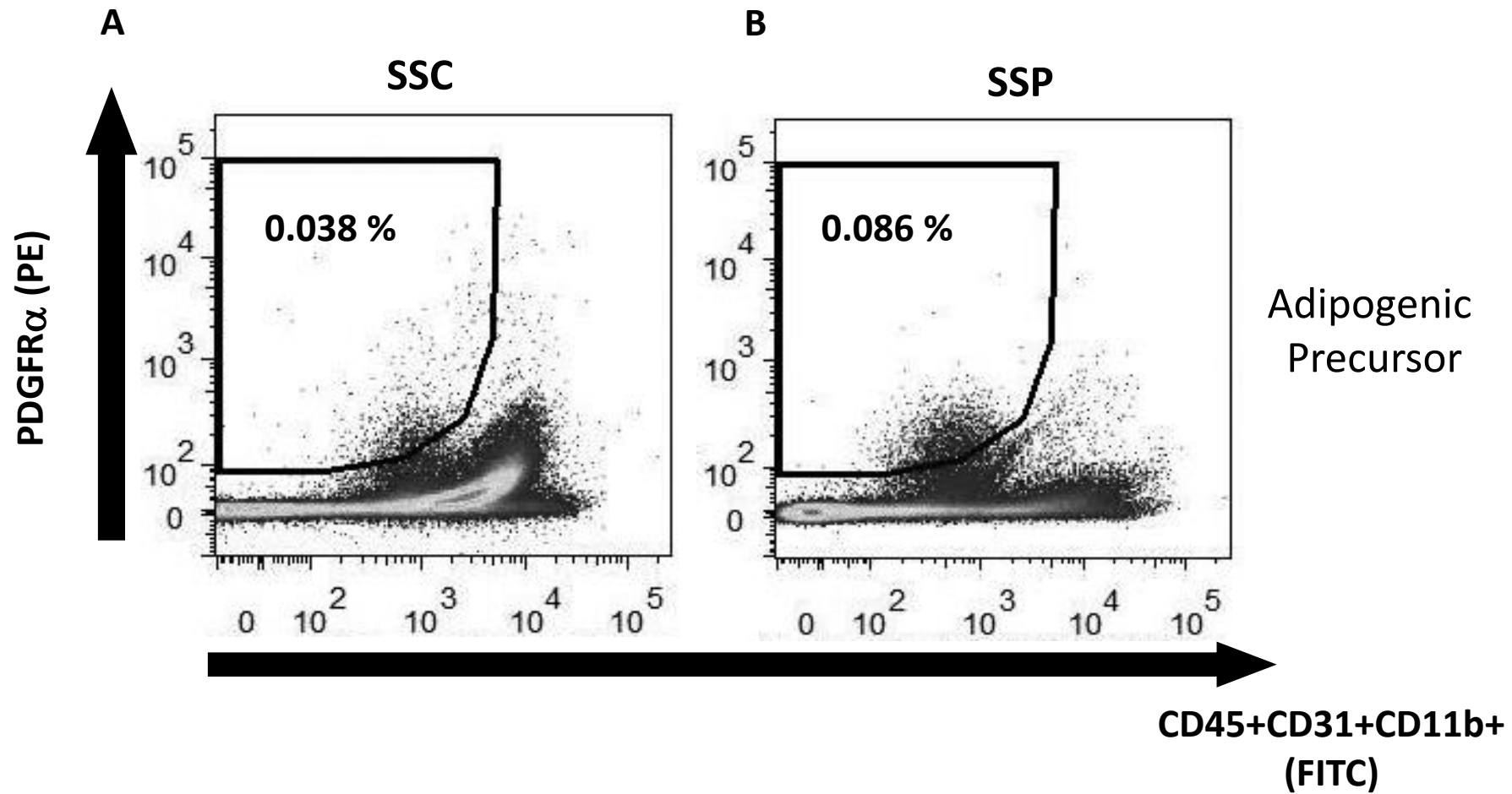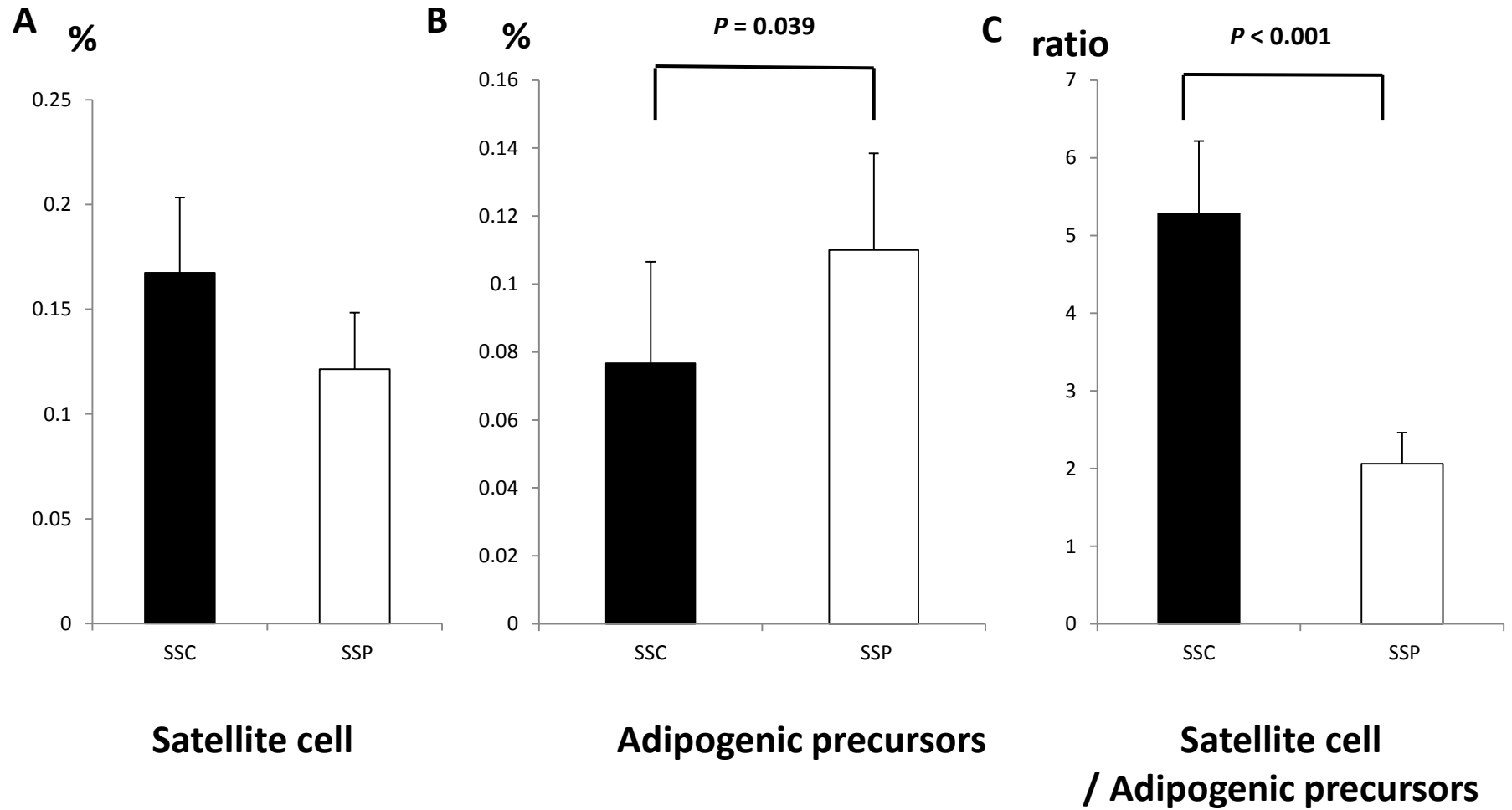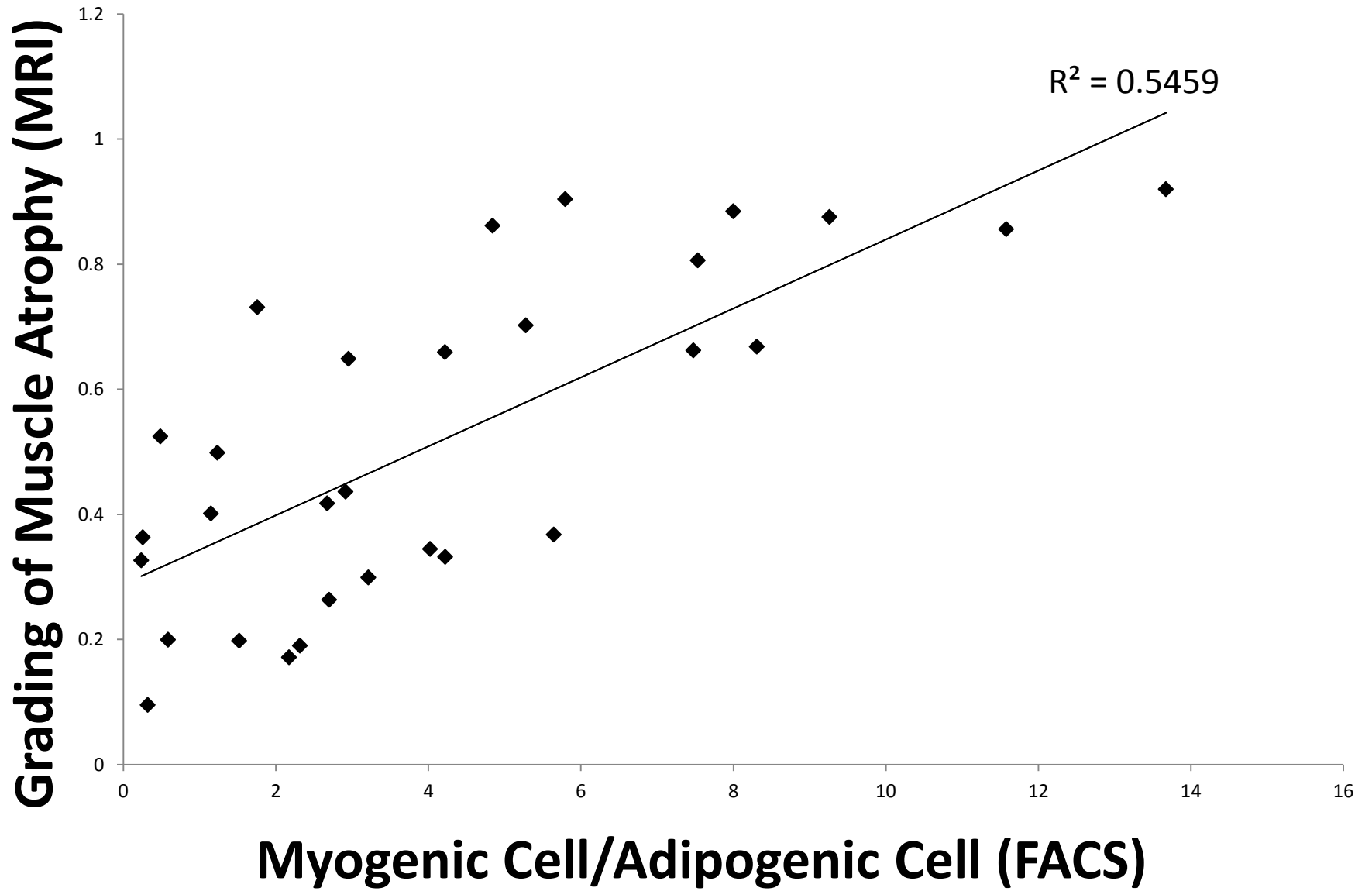
Fig. 11
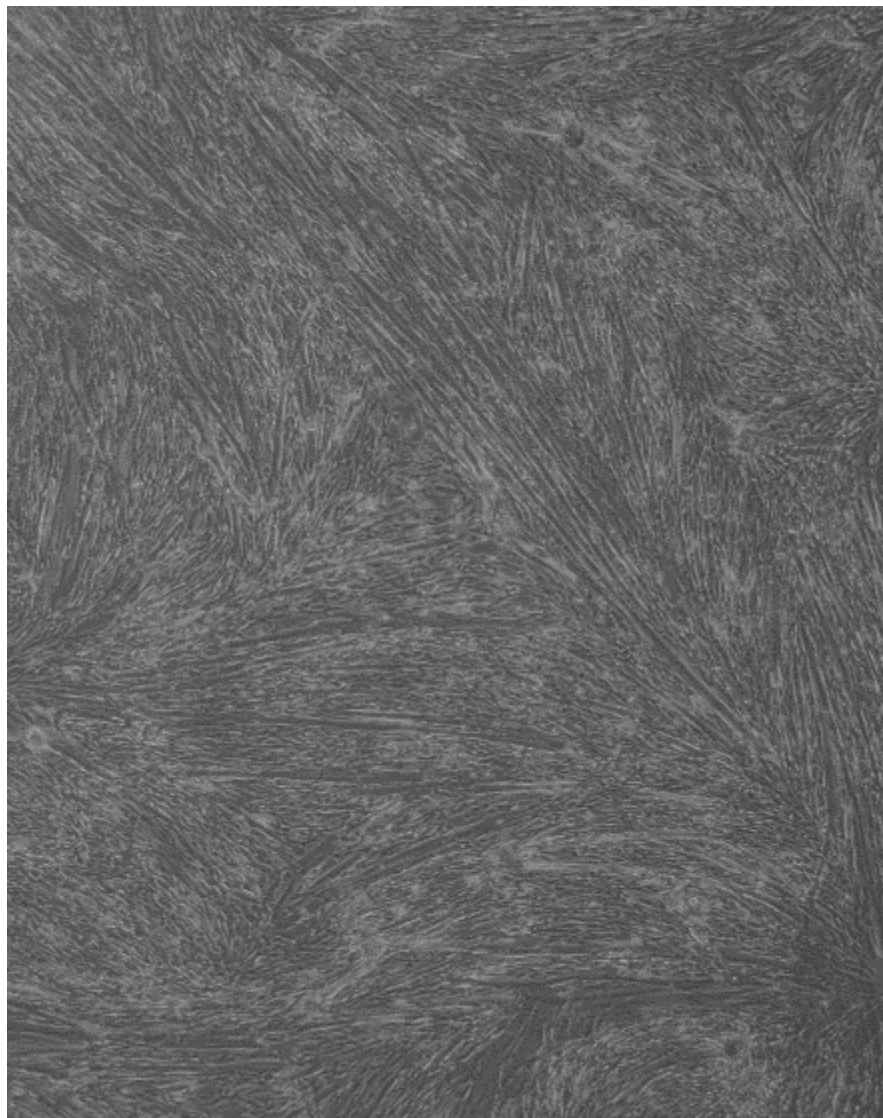
SSC
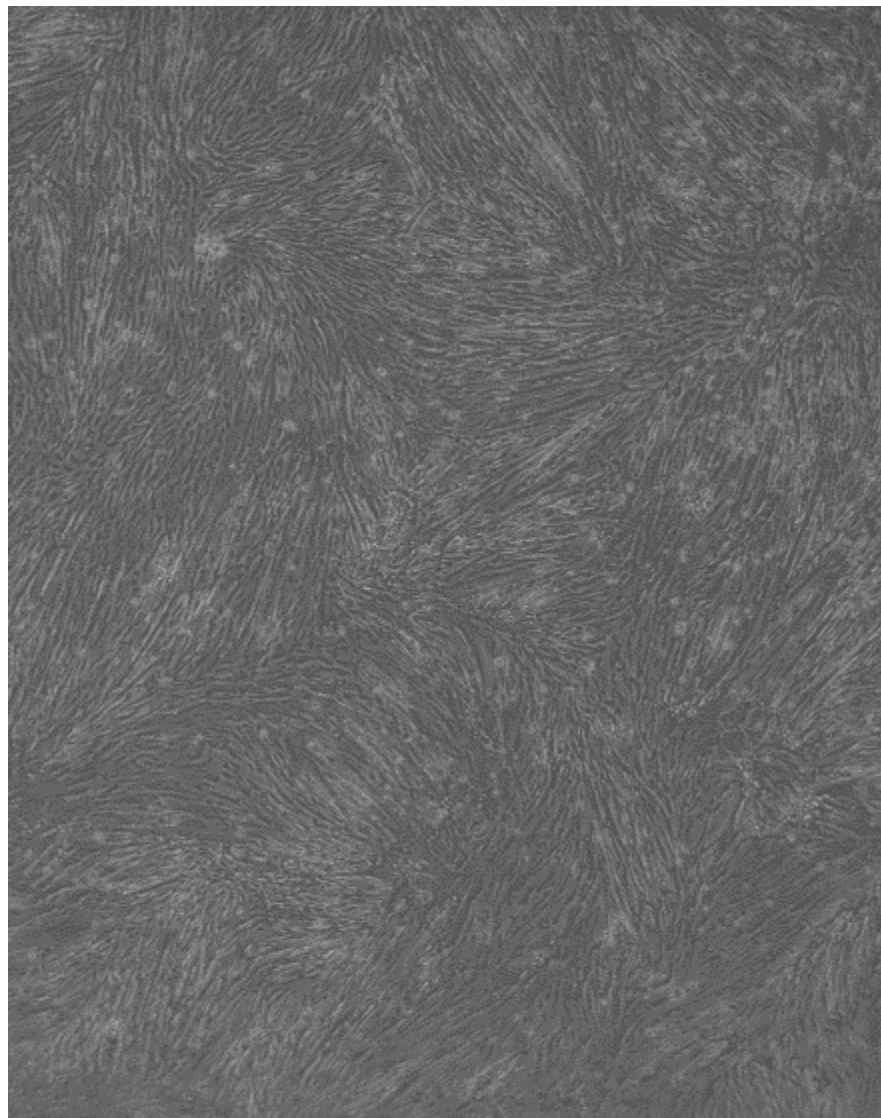
SSP

Fig. 12

SSC

SSP

Fig. 13

A

B
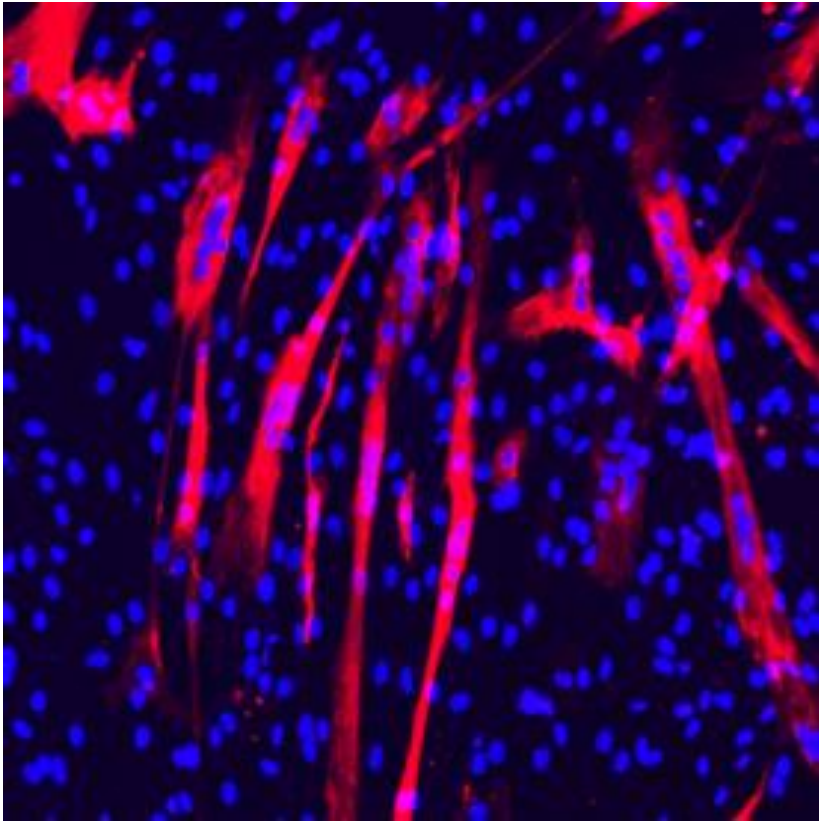
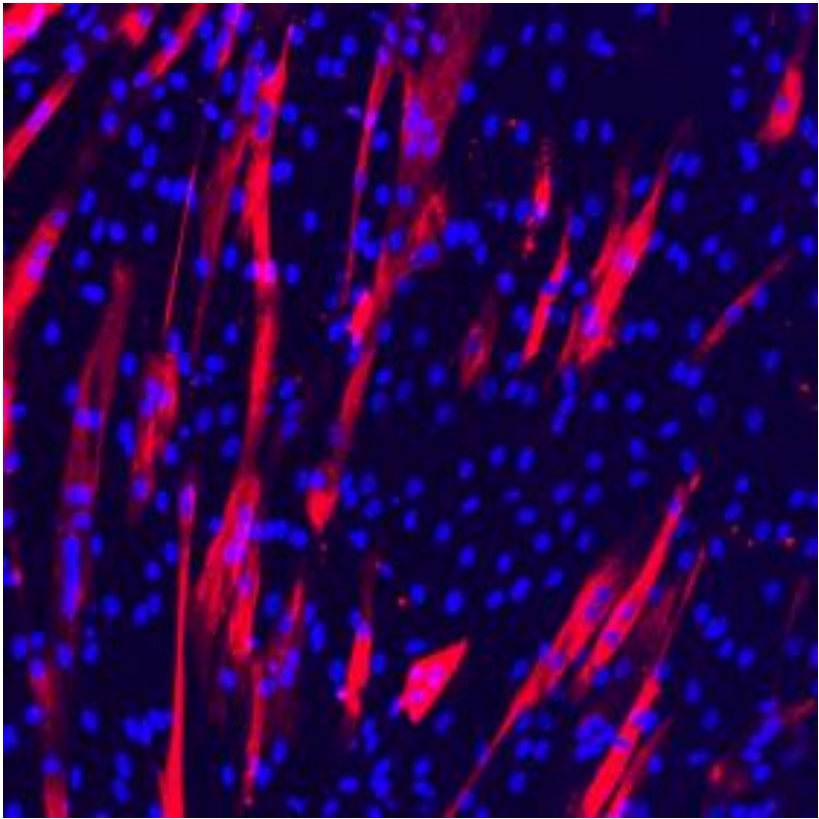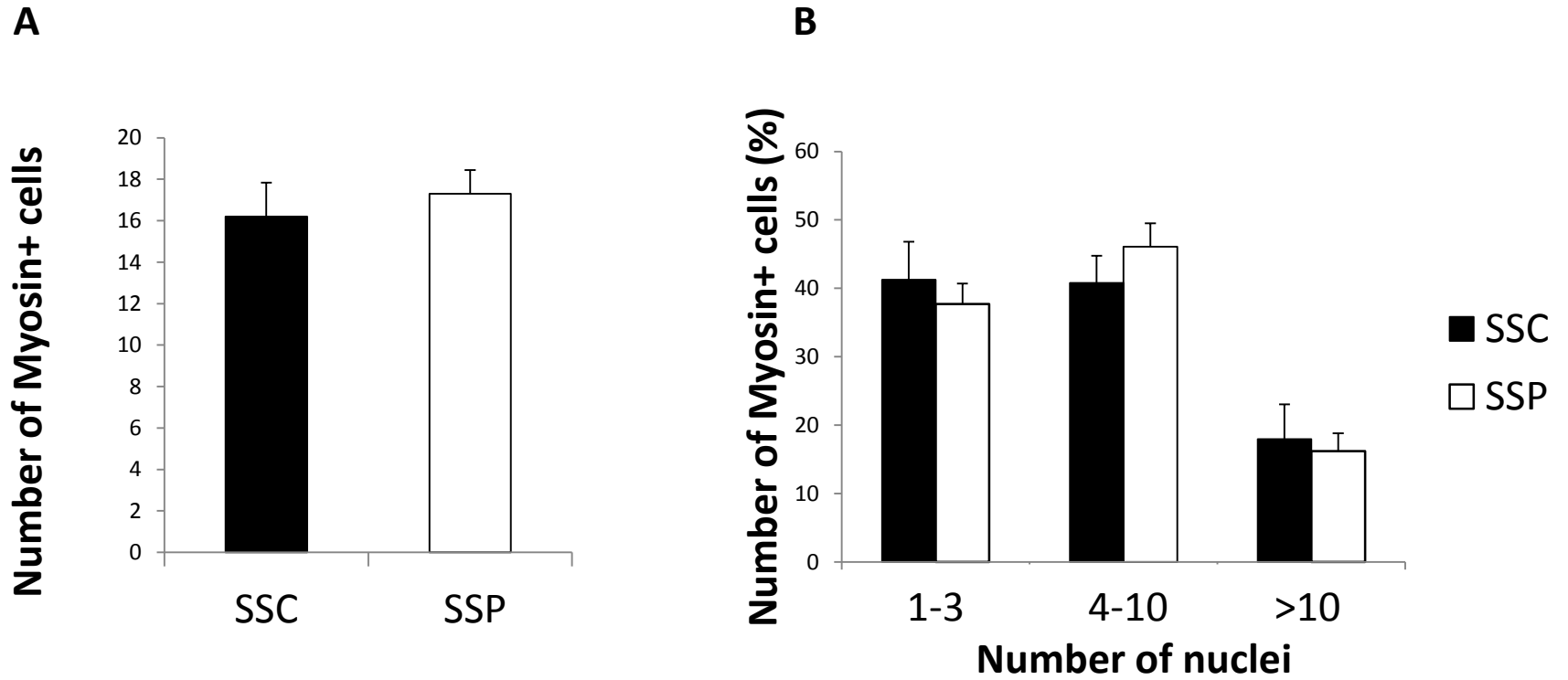**Table. 1**   **Recruited Patients' ID, Year, Sex, Tear size, and Goutallier classification (MRI)**

ID	Year	Sex	Tear Size	Goutallier Classification
1	71	F	Massive	4
2	47	M	Small	1
3	66	M	Massive	4
4	69	M	Massive	4
5	48	M	Massive	4
6	66	F	Massive	4
7	67	M	Massive	4
8	69	M	Medium	2
9	74	M	Large	3
10	61	F	Large	2
11	71	F	Medium	3
12	69	F	Massive	4
13	60	F	Large	2
14	68	M	Medium	3
15	69	F	Large	3
16	55	M	Large	4
17	60	M	Large	4
18	67	M	Large	3
19	76	F	Medium	4

Table. 2   **The Antibodies used for the Flowcytometry**

Antibody	Fluorecence	Cat. No.	Product	Dillution
anti-human CD140a(PDGFRα) Antibody	PE	323506	BioLegend	1:20
anti-human CD34 Antibody	PE/Cy7	343516	BioLegend	1:20
anti-human CD11b Antibody	FITC	301330	BioLegend	1:20
anti-human CD31 Antibody	FITC	303104	BioLegend	1:20
anti-human CD45 Antibody	FITC	304006	BioLegend	1:20
anti-human CD56(NCAM) Antibody	APC	304610	BioLegend	1:20
Human TruStain (Fc Receptor Blockin Solution)	None	422302	BioLegend	1:20
DAPI	DAPI	D212	Dojindo	1:1000

Table. 3   Increased Gene Profiles in SSP group compared with SSC group in microarray

GenBank	Gene Name	Description
NM_000041	ApoE	apolipoprotein E, mRNA
NM_017534	MYH2	myosin, heavy chain , skeletal muscle, adult, transcript variant 1, mRNA
NM_002422	MMP3	matrix metallopeptidase 3 (stromelysin 1, progelatinase), mRNA
NM_139250	CTAG1A	cancer/testis antigen 1A mRNA
NM_001102608	COL6A6	collagen, type VI, alpha 6, mRNA
NM_001025101	MBP	myelin basic protein, transient variant 7, mRNA
NM_014391	ANKRD1	ankyrin repeat domain 1,m RNA
NM_201442	C1S	complement component 1, s subcomponent, mRNA
NM_003857	BCAS1	breast carcinoma amplified sequence 1, mRNA
NM_005461	MAFB	v-mafavian musculoaponeurotic fibrosarcoma oncogene homolog B, mRNA
NM_001702	BAl1	brain-specific angiogenesis inhibitor 1, mRNA
NM_000104	CYP1B1	cytochrome P450, family 1, subfamily B, polypeptide 1, mRNA
NM_014059	RGCC	regulator of cell cycle, mRNA
NM_001033047	NPNT	nephronectin, transcript variant 2, mRNA
NM_006072	CCL26	chemokine ligand 26, mRNA
NM_002282	KRT83	keratin 83, mRNA
NM_005410	SEPP1	selenoprotein P, plasma 1, transcript variant 1, mRNA
NM_079420	MYL1	myosin, light chain 1, alkali: skeletal fast, transcript variant 1,mRNA
NM_000439	PCSK1	proprotein convertase subtilisin/kexin type 1,transcript variant 1, mRNA
NM_031455	CCDC3	coiled-coil domain containing 3, transcript variant 1, mRNA

Table. 4 **Decreased Gene Profiles in SSP group compared with SSC group in microarray**

GenBank	Gene Name	Description
NM_014620	HOX C4	homeobox C4, transcript variant 1, mRNA
NM_004503	HOX C6	homeobox C6, transcrpit variant 1, mRNA
NM_009586	SIM2	single-minded family bHLH transcription factor, transcript variant SIM2s, mRNA
NM_017541	CRYGS	crystalin, gamma S, mRNA
NM_000222	KIT	v-kit Hardy-Zuckeman 4 feline sarcoma viral oncogene homolog, transcript variant 1,mRNA
NM_000955	PTGER1	prostaglandin E receptor 1, mRNA
NM_015430	PAMR1	peptidase domain containing associated with muscle regeneration 1, transcript variant 1,mRNA
NM_020689	SLC24A3	solute carrier family 24, member 3, mRNA
NM_021013	KRT34	keratin 34, mRNA
NM_019605	SERTAD4	SERTA domain containing 4, mRNA
NM_005270	GLI2	GLI family zinc finger 2, mRNA
NM_026656	LOC400043	uncharacterized LOC40043, long non-coding RNA
NM_000217	KCNA1	potassium voltage-gated channel, shaker-related subfamily, member, mRNA
NM_005523	HOXA11	homeobox A11, mRNA
NM_002795	HOXA11-AS	HOXA11 antisense RNA, antisense RNA
NM_004101	F2RL2	coagulation factor II receptor-like 2, transcript variant 1,mRNA
NM_020639	RIPK4	receptor-interacting serine-threonine kinase 4, mRNA
NM_001164446	C6orfl32	chromosome 6 open reading frame 132, mRNA

Table. 5

Gene ontology analysis in SSP group compared with SSC group in microarray

Gene Ontology analysis with 20 up-regulated genes in SSP / SSC group				
GO ID	GO Term	all genes	hit genes	P-value
GO: 0044707	single-multicellular organism process	4561	14	1.66E-05
GO: 0030198	extracellular matrix organization	392	5	3.84E-05
GO: 0043062	extracellular structure organization	393	5	3.89E-05

Table. 6

Gene ontology analysis in SSP group compared with SSC group in microarray

Gene Ontology analysis with 18 down-regulated genes in SSP / SSC group				
GO ID	GO Term	all genes	hit genes	P-value
GO: 0007389	pattern specification process	449	5	1.58E-05
GO: 0001501	skeletal system development	488	5	2.35E-05
GO: 0009790	embryo development	870	6	2.75E-05
GO: 0060429	epithelium development	1083	6	9.36E-05